

**BRILLOUIN SCATTERING STUDIES IN LEAD
BISMUTH GALLATE BORON GLASSES**

By

SANG HOON PARK

Bachelor of Science

Hanyang University

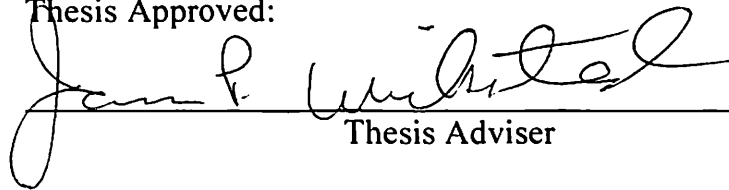
Seoul, Korea

2001

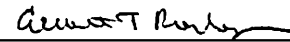
Submitted to the faculty of the
Graduate College of the
Oklahoma State University
in partial fulfillment of
the requirements for
the Degree of
MASTER OF SCIENCE
July, 2004


BRILLOUIN SCATTERING STUDIES IN LEAD
BISMUTH GALLATE BORON GLASSES

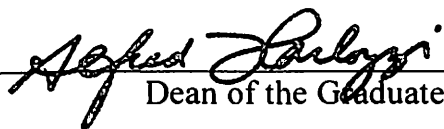
Thesis Approved:



Thesis Adviser







Dean of the Graduate College

ACKNOWLEDGMENTS

I wish to thank my dissertation advisor Dr. J.P. Wicksted for his advice, guidance, inspiration and support throughout this research project and study. I would also want to thank Dr. Shabbir M. Mian for preparing samples and Dr. Albert T. Rosenberger, Dr. Bret N. Flanders for serving on my thesis committee. I appreciate my parents.

TABLE OF CONTENTS

Chapter	Page
I .INTRODUCTION	1
Structure of samples.....	5
II. THEORY (Brillouin Light Scattering)	6
III. EXPERIMENTS.....	22
Samples preparation.....	22
BLS experiment and procedures.....	23
Refractive Index Measurements using a CCD.....	28
Density measurement.....	29
IV. RESULTS AND DISSCUSION.....	31
Brillouin shifts (ω_L).....	31
Elastic parameters.....	33
Photoelastic constants.....	35
Lorentz – Lorenz effect (LLE), Lattice effect (LE), Atomic effect (AE).....	37
Polarizability α	41
Correlation integral G.....	43
Absorption coefficients.....	45
VI. CONCLUSIONS AND FURTHER WORK.....	49
BIBLIOGRAPHY	

LIST OF TABLES

Table	Page
1. Composition of glass samples.....	3
2. Velocity, polarizations and BLS tensors for glasses.....	13
3. Brillouin shifts (ω_L), refractive indices n , and density ρ	31
4. Sound velocities and calculated elastic constants C_{11}	33
5. Photoelastic constants (P_{12}) vs. PbO mole%.....	35
6. Lorentz – Lorenz effect (LLE), Lattice effect (LE), Atomic effect (AE) contribution to the photoelastic constants (P_{12}).....	37
7. Polarizability α	41
8. The correlation integral G.....	43
9. Absorption coefficients ($\alpha_{absorption}$).....	45

LIST OF FIGURES

Figure	Page
1. Brillouin light scattering process.....	7
2. Right-angle Bragg diffraction by sound waves in the glass (sample).....	12
3. Polarized BLS spectra of PbO.0.46 glass.....	19
4. The absorption measurement.....	21
5. 6-pass tandem Fabry-Perot interferometer.....	25
6. Optics and optical pathways within 6-pass tandem Fabry-Perot interferometer.....	26
7. Top view of the sample for the incident and scattered light distance.....	27
8. Setup for refractive index measurements.....	30
9. Brillouin spectra of lead bismuth boron gallate glasses.....	32
10. Calculated elastic constants (C_{11}) vs. PbO mole %.....	34
11. Calculated photoelastic constants (P_{12}) vs. PbO mole %.....	36
12. Lorentz – Lorenz effect (LLE) vs. PbO mole %.....	38
13. Lattice effect (LE) vs. PbO mole %.....	39
14. Atomic effect (AE) vs. PbO mole %.....	40
15. Polarizability α vs. PbO mole %.....	42
16. The correlation integral G vs. PbO mole %.....	44
17. Absorption coefficients ($\alpha_{absorption}$) vs. PbO mole %.....	46

Chapter I

Introduction

The focus of this dissertation is to study the optical properties (measurements of elastic and photoelastic constants) of lead bismuth gallate boron glasses. Over the past three decades, there has been significant fundamental interest in the optical properties of glasses motivated by the desire to use glasses in photonics applications. Unfortunately, the basic physics behind certain aspects of glass optical properties remains unclear such as the role of network formers and modifiers. Our goal is to experimentally investigate the role lead and bismuth play in enhancing the optical properties of lead-bismuth-gallates and experimentally investigate optical properties of a relatively new family of heavy-metal oxide glasses called lead-bismuth-gallates-boron. These glasses were first introduced about 15 years ago within the context of producing glasses that are highly transparent in the infrared region of the spectrum [1]. Previous optical studies on lead-bismuth-gallates have been few in number and limited to similar compositions [2-4]. The effect of the network modifying and network forming capabilities of lead and bismuth on enhancing the optical properties in these glasses is unclear. To address this issue, we will change the lead and bismuth content of the lead-bismuth-gallates-boron systematically in our study.

We plan to investigate six samples of lead-bismuth-gallates-boron with compositions $\text{PbO} (x) - \text{BiO}_{1.5} (0.7-x) - \text{GaO}_{1.5} (0.3) - \text{B}_2\text{O}_3 (0.8)$, where $x = 0.7, 0.62, 0.46, 0.31, 0.16, 0$ in mole fraction (See table 1). This particular compositional variation,

where the glass system is taken from a pure lead gallate to a pure bismuth gallate, while keeping the heavy metal concentration (Pb^{2+} or Bi^{3+}) constant, will allow us to study the optical effects of both the network forming and network modifying capabilities of lead and bismuth. At high concentrations (over 0.30), both PbO and Bi_2O_3 will behave as network formers, in which case the other heavy metal constituent (Pb^{2+} or Bi^{3+}) will act as a network modifier [5]. We will perform Brillouin scattering measurements in order to determine the optical properties for the lead bismuth gallate boron glasses. This will allow us to study the optical effects of both the network forming and network modifying capabilities of lead and bismuth.

Brillouin scattering studies will provide information about the elastic and photoelastic properties as well as the general structural bonding information for these glasses. For the experiment, we will use a right-angle scattering geometry along with an Argon 514.5 nm line (single-longitudinal mode), and a Multi-Pass Tandem Fabry-Perot Interferometer. Since optical properties scale with heavy metal content, our study should provide information on the role lead and bismuth play structurally. By performing the experiments at 514.5 nm, we will test for dispersion in the optical properties. The linear absorption edges and refractive indices of the glasses will be measured using a spectrometer and the Brewster's angle method [6]. To our knowledge, this is the first systematic exploration of the role lead and bismuth play in the optical properties of bismuth gallate boron glasses. We believe the knowledge gained in investigating the effect of glass structure to optical properties is applicable to other fields such as semiconductors, organics.

Sample ID	PbO (mole%)	Bi₂O₃ (mole%)	Ga₂O₃ (mole%)	B₂O₃ (mole%)
PbO.0 Bi₂O₃.0.62	0	62	30	8
PbO.0.16 Bi₂O₃.0.46	16	46	30	8
PbO.0.31 Bi₂O₃.0.31	31	31	30	8
PbO.0.46 Bi₂O₃.0.16	46	16	30	8
PbO.0.62 Bi₂O₃.0	62	0	30	8
PbO.0.70 Bi₂O₃.0	70	0	30	0

Table 1. Composition of glass samples

Structure of samples

The structure of $PbO-BiO_{1.5}-GaO_{1.5}$ glasses has been investigated by IR and Raman spectroscopy which were done by Fumiaki Miyaji and Sumio Sakka [5]. An infrared absorption band involving four-coordinated Ga^{3+} ions was observed at above 610-650 cm^{-1} . This band peak shifts toward higher wavenumbers with increasing $GaO_{1.5}$ content, indicating that covalency of $Ga-O$ bond increases with increasing $GaO_{1.5}$ content. Raman studies indicate bands at about 130 cm^{-1} , 400 cm^{-1} , 550 cm^{-1} and 650 cm^{-1} which have been assigned to $Pb-O$ or $Bi-O$, $Ga-O-Pb$ or $Ga-O-Bi$, $Ga-O-Ga$, and $Ga-O_{non-bridging}$ vibrations, respectively. The fraction of non-bridging oxygen in GaO_4 tetrahedra decreases with increasing PbO and $BiO_{1.5}$ concentrations. It is assumed that most Pb^{2+} and Bi^{3+} ions are network formers.

The Raman scattering cross-section and non-linear optical response of lead borate glasses were done by Zhengda Pan, Steven H. Morgan, and Bryan H. Long [7]. Lead borate glasses in the system $xPbOg(10-x)B_2O_3$ ($5 \leq x \leq 9$) have been studied by Raman scattering and Z-scan non-linear optical measurements. It is found that both the Raman scattering cross-section and non-linear refractive index, n_2 , of the glasses increase significantly with increasing lead oxide content. The increase in Raman cross-section is dominated by an increase in the low-frequency Raman scattering. The results indicate that both electronic and nuclear responses contribute to the observed optical non-linearity which is further enhanced by two-photon resonance effects for glasses with $x \geq 80$ mole%. The nuclear is attributed to low-frequency vibrational modes and the electronic response to highly polarizable lead cations in the glass matrix.

The Neutron and X-ray diffraction studies of $PbO-Ga_2O_3$ and $Bi_2O_3-Ga_2O_3$ glasses were done by Fumiaki Miyaji, Toshinobu Yoko, Jisun Jin, Sumio Sakka, Toshiharu Fukunaga, Masakatsu Misawa [8]. The structure of $50PbO-50GaO_{1.5}$ and $80BiO_{1.5}-20GaO_{1.5}$ glasses was investigated by neutron and X-ray diffraction. Most Ga^{3+} ions are four-coordinated in both glasses. The stronger glass-forming ability in $PbO-GaO_{1.5}$ is attributed to $(PbO_3, PbO_4)_n$ infinite spiral chains as in crystalline $PbSiO_3-Bi^{3+}$ ions form BiO_5 and BiO_6 units in $80BiO_{1.5}-20GaO_{1.5}$ glass as in $\alpha - Bi_2O_3$. This glass may be constructed by $(PbO_5, PbO_6)_n$ layers and GaO_3^{3-} chains.

Chapter II
Brillouin Scattering
Theory

Brillouin light spectroscopy (BLS) is an important light scattering procedure which was first pointed out by L. Brillouin in 1922 [9]. Brillouin scattering could not be broadly used because of the lack of coherent light sources until the laser was discovered in 1960. The inelastic scattering of photons from thermally excited acoustic phonons results in the Brillouin scattering phenomenon. An important point of BLS is that the technique does not require mechanical contact. The acoustic phonons act as propagating density gratings which diffract and Doppler shift the laser light.

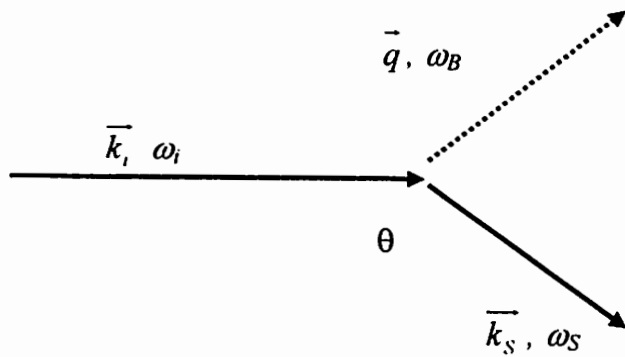
Brillouin light scattering can be explained by either a classical or quantum mechanical point of view. In the quantum point of view, there are two cases; creation (Stokes event) or destruction (anti-Stokes event) of a phonon (see Fig.1).

From the energy and momentum conservation:

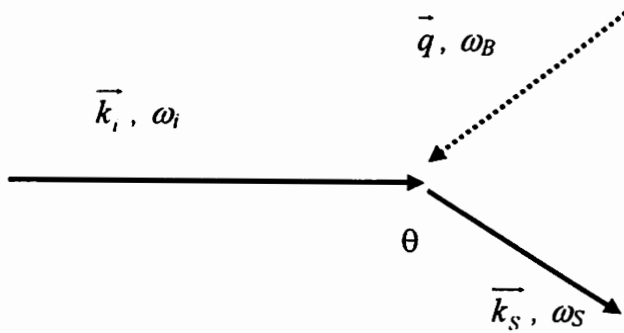
$$\omega_s = \omega_i \pm \omega_B \quad (2.1)$$

$$\vec{k}_s = \vec{k}_i \pm \vec{q} \quad (2.2)$$

where an incident photon wavevector \vec{k}_i and frequency ω_i is scattered into wavevector \vec{k}_s and frequency ω_s during the interaction a phonon wavevector \vec{q} and frequency ω_B (Brillouin shift).



(a) Phonon Creation (Stokes event)



(b) Phonon Destruction (anti-Stokes event)

Fig . 1. Brillouin light scattering process.

Elastic scattering occurs with $\omega_s = \omega_i$ and there is no phonon involvement. Brillouin shifts ω_B are very small (on the order of 10 GHz) compared to incident and scattered light frequencies.

The wave vector of acoustic phonon

$$|q| = |\vec{k}_i - \vec{k}_s| = 2n|\vec{k}_i| \sin\left(\frac{\theta}{2}\right) \quad (2.3)$$

where θ and n are the scattering angle and the index of refraction of the sample.

We can get the sound velocity from (2.1), (2.2), and (2.3):

$$v = \frac{\omega_B}{q} = \frac{\omega_B}{2n|\vec{k}_i| \sin\left(\frac{\theta}{2}\right)} = \frac{\omega_B \lambda_i}{4\pi n \sin\left(\frac{\theta}{2}\right)} \quad (2.4)$$

where ω_B is the Brillouin shift in rad/sec units and λ_i is the incident light wavelength.

We consider the equation of motion for an elastic medium. In crystal lattice dynamics, the stress is as follows:

$$S_{ik} = C_{iklm} \frac{\partial u_m}{\partial r_l} \quad (2.5)$$

where C_{iklm} is the elastic stiffness tensor. The equation of motion in the harmonic approximation is as follows:

$$\rho \frac{\partial^2 u_i}{\partial t^2} = \frac{\partial S_{ik}}{\partial r_k} = C_{iklm} \frac{\partial^2 u_m}{\partial r_k \partial r_l} \quad (2.6)$$

Here u is the displacement vector, ρ is the density, and r is the location of the equilibrium point that is being displaced

Assuming the plane-wave solution of the following form:

$$u_m = u_m^0 e^{i(\vec{q} \cdot \vec{r} - \omega t)} \quad (2.7)$$

and substituting (2.7) into (2.6) we get:

$$\rho\omega^2 u_i^0 = C_{iklm} q_k q_l u_m^0$$

or,

$$\left[C_{iklm} q_k q_l - \rho\omega^2 \delta_{im} \right] u_m^0 = 0 \quad (2.8)$$

If the wavelength is very long, then $\omega_B = vq$, where v is the appropriate sound velocity.

$$\text{Therefore, } \sum_{kl} \left[C_{iklm} \hat{q}_k \hat{q}_l - \rho v^2 \delta_{im} \right] u_m^0 = 0 \quad (2.9)$$

where $\hat{q}_k = \frac{q_k}{|q|}$ is the k-component of unit vector \hat{q} . For non-trivial solutions (2.9) the

secular determinant has to vanish. The non-zero elastic constants are conditional on the symmetry of the material.

For an isotropic medium like glass, the form of the elastic constant (C_{mn}) matrix is as follows [10]:

$$C_{mn} = \begin{bmatrix} C_{11} & C_{12} & C_{12} & 0 & 0 & 0 \\ C_{12} & C_{11} & C_{12} & 0 & 0 & 0 \\ C_{12} & C_{12} & C_{11} & 0 & 0 & 0 \\ 0 & 0 & 0 & \frac{1}{2}(C_{11}-C_{12})=C_{44} & 0 & 0 \\ 0 & 0 & 0 & 0 & \frac{1}{2}(C_{11}-C_{12})=C_{44} & 0 \\ 0 & 0 & 0 & 0 & 0 & \frac{1}{2}(C_{11}-C_{12})=C_{44} \end{bmatrix} \quad (2.10)$$

For isotropic media, the stress is proportional to a small strain which requires two independent elastic constants C_{11} and C_{44} . The third elastic constant C_{12} is $C_{11} - 2C_{44}$ by the Cauchy relation [11]. If the wavevector \hat{q} propagates in the [1,0,0] direction, Then using the matrix (2.10), we can get the following eigenvalues and eigenvectors:

$$\rho v_l^2 = (\omega^2 \rho)_1 = (v^2 \rho)_1 = C_{11}, \quad \vec{u} = (1,0,0) \quad (2.11a)$$

$$\rho v_{T1}^2 = (\omega^2 \rho)_2 = (v^2 \rho)_2 = C_{44}, \quad \vec{u} = (0,1,0) \quad (2.11b)$$

$$\rho v_{T2}^2 = (\omega^2 \rho)_3 = (v^2 \rho)_3 = C_{44}, \quad \vec{u} = (0,0,1) \quad (2.11c)$$

where \vec{u} is the unit vector of the displacement direction and \hat{q} is the direction of sound wave propagation. The equation (2.11a) is equivalent to the longitudinal mode and the equation (2.11b) and equation (2.11c) are equivalent to the transverse modes.

We can calculate the elastic constants C_{11} (longitudinal mode) and C_{44} (transverse mode) from equation (2.4) and equation (2.11):

$$C_{11} = \rho v_l^2 = \frac{\rho \omega_l^2 \lambda_l^2}{4n^2 \sin^2\left(\frac{\theta}{2}\right)} \quad (2.12a)$$

$$C_{44} = \rho v_T^2 = \frac{\rho \omega_T^2 \lambda_T^2}{4n^2 \sin^2\left(\frac{\theta}{2}\right)} \quad (2.12b)$$

The glasses have Brillouin peaks and a Rayleigh line. These Brillouin peaks correspond to both a transverse and longitudinal phonon, which can be separated utilizing distinct polarizations of the incident and scattered light. The intensity of the Brillouin peak is also an important component. The sound wave produces a local strain in the material which in turn perturbs the local dielectric constant ε by an increment $\delta\varepsilon$. A plane monochromatic wave across the material will cause this perturbation $\delta P = E_0 \delta\varepsilon / 4\pi$ which is an additional polarization and will scatter light at shifted frequencies corresponding to the acoustic modes. For incident light polarized in the j -th direction and scattered light polarized in the i -th direction, the Rayleigh ratio, or differential cross-section per unit volume of the glass is:

$$R_y = \frac{r^2 I'_s}{\Delta\Omega \cdot \Lambda I'_i} = \frac{r^2 I'_s}{\Delta\Omega \cdot LP'_i} \quad (2.13)$$

where r^2 is the squared distance from the scattering volume to the detector, Λ is the scattering volume from which light is being collected, $\Delta\Omega$ is the solid angle in the air at which the scattering volume is collected, I_i and I_s are the incident and scattered intensities. LP'_i is used instead of $\Lambda I'_i$ where L is the length of the scattering column from which light is being collected and P'_i is the measurable incident power. The local strain tensor x_{kl} and the change in the reciprocal dielectric constant $\Delta(\epsilon^{-1})_{ij}$ induced is governed by the photoelastic constants (Pockel's coefficients) p_{ijkl} through the following linear relation:

$$\Delta(\epsilon^{-1})_{ij} = \sum_{kl} p_{ijkl} x_{kl} \quad (2.14)$$

If we assume that the each acoustic mode excitation is on an average in thermal equilibrium at temperature T , then the Rayleigh ratio is given by [12]:

$$R^j = \frac{k_B T \omega_s^4}{32\pi^2 c^4 \rho v_j^2} [\hat{e}_s \cdot \vec{T}^j \cdot \hat{e}_i]^2 (n_s / n_i) \quad (2.15)$$

where v_j is the velocity of the j_{th} acoustic mode and ω_s is the frequency of the scattered light, \vec{T}^j is the Brillouin tensor for the j_{th} direction, \hat{e}_s and \hat{e}_i are the polarization directions of the scattered and incident light. Now, for an isotropic medium, the refraction indices of the propagation of scattered light n_s and refraction indices of the propagation of incident light n_i are identical. For numerous crystal classes, Cummins and Schoen [12] tabulated Brillouin tensors including those for an isotropic glass. The Bragg diffraction of incident light by propagating sound waves in the glass is illustrated in Fig 2.

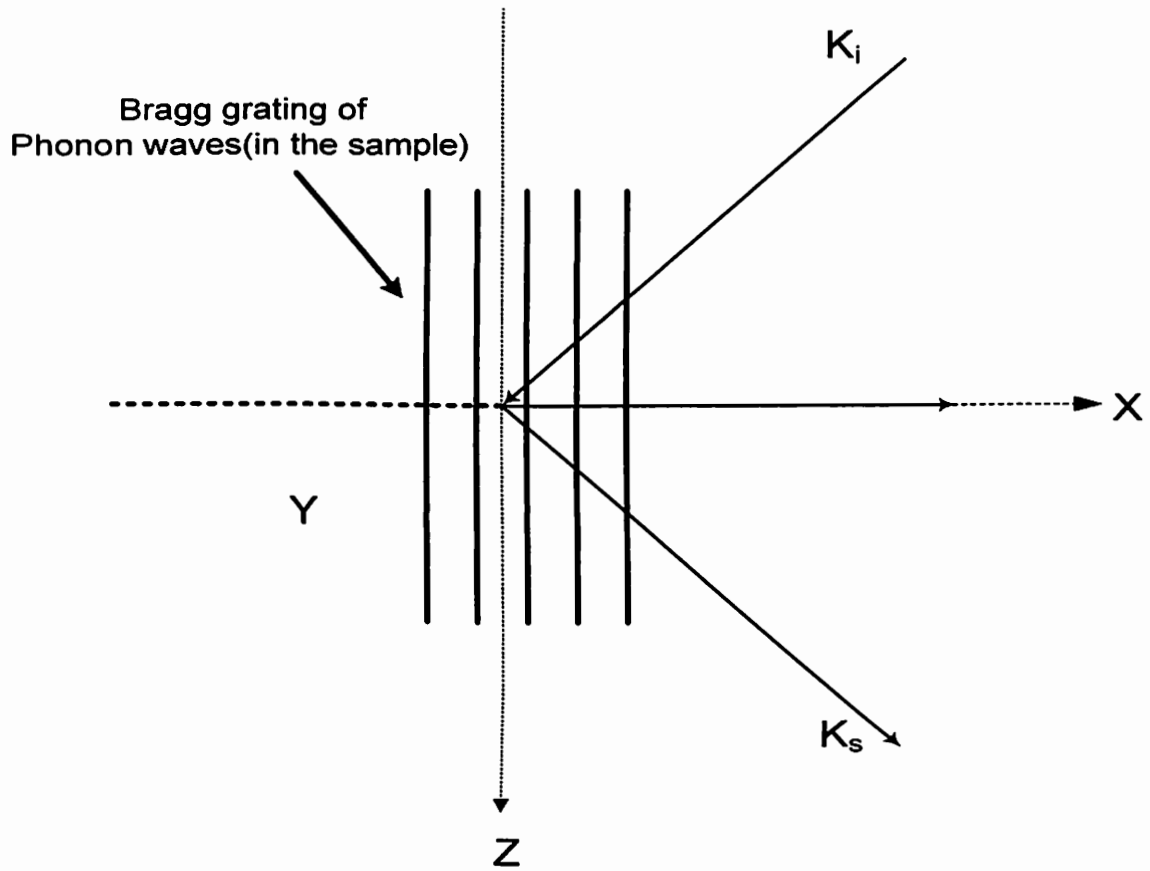


Fig. 2. Right-angle Bragg diffraction by sound waves in the glass (sample).

$$\rho v_l^2 = C_{11} \quad : \quad \hat{u} = (1,0,0) \text{ Longitudinal}$$

$$\vec{T} = \varepsilon^2 \begin{pmatrix} P_{11} & 0 & 0 \\ 0 & P_{12} & 0 \\ 0 & 0 & P_{12} \end{pmatrix}$$

$$\rho v_r^2 = \frac{1}{2}(C_{11} - C_{12}) = C_{44} \quad : \quad \hat{u} = (0,1,0) \text{ Transverse}$$

$$\vec{T} = \varepsilon^2 \begin{pmatrix} 0 & \frac{1}{2}(P_{11} - P_{12}) & 0 \\ \frac{1}{2}(P_{11} - P_{12}) & 0 & 0 \\ 0 & 0 & 0 \end{pmatrix}$$

$$\rho v_r^2 = \frac{1}{2}(C_{11} - C_{12}) = C_{44} \quad : \quad \hat{u} = (0,0,1) \text{ Transverse}$$

$$\vec{T} = \varepsilon^2 \begin{pmatrix} 0 & 0 & \frac{1}{2}(P_{11} - P_{12}) \\ 0 & 0 & 0 \\ \frac{1}{2}(P_{11} - P_{12}) & 0 & 0 \end{pmatrix}$$

Table 2. Velocity, polarizations and BLS tensors for glasses

(The Brillouin scattering tensors are listed for (1,0,0), (0,1,0) and (0,0,1) acoustic)

From the incident and scattered light, if the vertical polarization is in y-direction and horizontal polarization is in xz – plane, we can get a total of four possible polarization directions.

1) Incident light vertically polarized : $\hat{e}_i = \begin{pmatrix} 0 \\ 1 \\ 0 \end{pmatrix}$,

2) Incident light horizontally polarized : $\hat{e}_i = \frac{1}{\sqrt{2}} \begin{pmatrix} 1 \\ 0 \\ 1 \end{pmatrix}$,

3) Scattered light vertically polarized : $\hat{e}_s = (010)$

4) Scattered light horizontally polarized : $\hat{e}_s = \frac{1}{\sqrt{2}}(10\bar{1})$.

The four possibilities for these four combinations of $[\hat{e}_s \cdot \vec{T}' \cdot \hat{e}_i]$:

VV:

$$(0 \ 1 \ 0) \epsilon^2 \begin{pmatrix} P_{11} & 0 & 0 \\ 0 & P_{12} & 0 \\ 0 & 0 & P_{12} \end{pmatrix} \begin{pmatrix} 0 \\ 1 \\ 0 \end{pmatrix} = \epsilon^2 P_{12} \quad (2.16a)$$

HH:

$$(1 \ 0 \ \bar{1}) \frac{1}{\sqrt{2}} \epsilon^2 \begin{pmatrix} P_{11} & 0 & 0 \\ 0 & P_{12} & 0 \\ 0 & 0 & P_{12} \end{pmatrix} \frac{1}{\sqrt{2}} \begin{pmatrix} 1 \\ 0 \\ 1 \end{pmatrix} = \frac{1}{2} \epsilon^2 (P_{11} - P_{12}) = \frac{1}{2} \epsilon^2 P_{44} \quad (2.16b)$$

VH:

$$(1 \ 0 \ \bar{1}) \frac{1}{\sqrt{2}} \varepsilon^2 \begin{pmatrix} 0 & \frac{1}{2}(P_{11} - P_{12}) & 0 \\ \frac{1}{2}(P_{11} - P_{12}) & 0 & 0 \\ 0 & 0 & 0 \end{pmatrix} \begin{pmatrix} 0 \\ 1 \\ 0 \end{pmatrix} = \frac{\varepsilon^2}{2\sqrt{2}} (P_{11} - P_{12}) = \frac{1}{\sqrt{2}} \varepsilon^2 P_{44} \quad (2.16c)$$

HV:

$$(0 \ 1 \ 0) \frac{\varepsilon^2}{\sqrt{2}} \begin{pmatrix} 0 & \frac{1}{2}(P_{11} - P_{12}) & 0 \\ \frac{1}{2}(P_{11} - P_{12}) & 0 & 0 \\ 0 & 0 & 0 \end{pmatrix} \begin{pmatrix} 1 \\ 0 \\ 1 \end{pmatrix} = \frac{\varepsilon^2}{2\sqrt{2}} (P_{11} - P_{12}) = \frac{1}{\sqrt{2}} \varepsilon^2 P_{44} \quad (2.16d)$$

To select V - polarization or H - polarization for the incident light, a polarization rotator is mounted to the laser head and to select V - polarization or H - polarization for the scattering Brillouin light, a polarization analyzer is placed in front of the 6-pass Fabry-Perot Interferometer. We can compare experimental results of the Brillouin intensities with the theoretical results of Equation (2.16). VV polarization is used to select pure longitudinal acoustic phonons. On the other hand, VH and HV polarizations select pure transverse acoustic phonons in Fig 3. Crossing VV+VH polarization is the superposition of VV plus VH modes.

Using the right scattering angle geometry ($\theta = 90^\circ$) with $\omega_s \approx \omega_i$, and $\varepsilon = n^2$, the polarization selection $[\hat{e}_s \cdot \vec{T}^j \cdot \hat{e}_i]$ -values (2.16) are substituted into the Rayleigh ratio (2.15). From equation (2.12), we will get the following relations for the absorption-free integrated Brillouin scattering intensities:

$$I_{VV} = \left(\frac{\Delta\Omega}{r^2} \right) (P_i L_{eff}) \left(\frac{\omega_i}{c} \right)^6 \left(\frac{k_B T}{\pi^2} \right) \left(\frac{n^{10}}{\rho \omega_i^2 (n+1)^4} \right) P_{12}^2 \quad (2.17a)$$

$$I_{HH} = \left(\frac{\Delta\Omega}{2r^2} \right) (P_i L_{eff}) \left(\frac{\omega_i}{c} \right)^6 \left(\frac{k_B T}{\pi^2} \right) \left(\frac{n^{10}}{\rho \omega_i^2 (n+1)^4} \right) (P_{11} - P_{12})^2 \quad (2.17b)$$

$$I_{HV} = I_{VH} = \left(\frac{\Delta\Omega}{2r^2} \right) (P_i L_{eff}) \left(\frac{\omega_i}{c} \right)^6 \left(\frac{k_B T}{\pi^2} \right) \left(\frac{n^{10}}{\rho \omega_i^2 (n+1)^4} \right) P_{44}^2 \quad (2.17c)$$

Here, the factor $16n^2/(n+1)^2$ results from the transmission of the incident laser beam into the sample and includes the effective solid angle $\frac{\Delta\Omega}{n^2}$ correction from the material [13,14].

Photoelastic constants are hard to measure from equation (2.17), so we use the absolute measurement of the scattering intensities. That is, the Brillouin scattering intensities for the longitudinal and transverse Brillouin components on our samples are measured relative to a fused quartz standard with known photoelastic constants:

$$P_{12} = \left(\frac{n^0}{n} \right)^5 \left(\frac{n+1}{n^0+1} \right)^2 \left(\frac{\omega_i}{\omega_i^0} \right) \left(\frac{\rho I_L(VV)}{\rho^0 I_L^0(VV)} \right)^{1/2} P_{12}^0 \quad (2.18a)$$

$$P_{44} = \left(\frac{n^0}{n} \right)^5 \left(\frac{n+1}{n^0+1} \right)^2 \left(\frac{\omega_T}{\omega_T^0} \right) \left(\frac{\rho I_T(VH)}{\rho^0 I_T^0(VH)} \right)^{1/2} P_{44}^0 \quad (2.18b)$$

where $I_L(VV)$ is the integrated intensity of longitudinal mode and $I_T(VH)$ integrated intensity of transverse mode. The measured values for the standard sample (fused quartz) are labeled with superscript "0". The air temperature T , laser frequency ω_i , laser power P_i , collection solid angle $\Delta\Omega$, scattering angle ($\theta = 90^\circ$), the effective scattering column length (L_{eff}), and the distance r from the sample's scattering column

to the PMT are fixed. Carleton [15] and Matusita [16] suggested the Pockels elastooptic constants P_{12} and P_{44} for amorphous solids can be expressed as follows [11, 17]:

$$\begin{aligned}
 P_{12} &= \left(\frac{(n^2-1)^2}{n^4} \times \frac{M}{4\pi\alpha\rho N_A} \right) - \left(\frac{(n^2-1)^2}{n^4} \times \frac{2}{15} \right) - \left(\frac{(n^2-1)^2}{n^4} \times \frac{8}{15} \times 3\alpha G \right) \\
 &= \text{LLE} + \text{LE} + \text{AE}
 \end{aligned} \tag{2.19}$$

$$\begin{aligned}
 P_{44} &= \frac{(n^2-1)^2}{5n^4} - \left(\frac{(n^2-1)^2}{5n^4} \times 3\alpha G \right) \\
 &= -\frac{3}{2}\text{LE} + \frac{3}{8}\text{AE}
 \end{aligned} \tag{2.20}$$

where n is the index of refraction, α is the glass average polarization, ρ is the particle density, M is the molecular weight of the glass, N_A is the Avogadro's number.

The correlation integral G is given by

$$G = \int_0^{\infty} dr \frac{g_{12}(r)}{r^4} \tag{2.21}$$

where $g_{12}(r)$ is a two-particle radial distribution function. The Photoelastic constant P_{44} does not depend directly on density. The reason is that an average displacement among neighboring atoms in the perpendicular direction of the compressional sound wave is negligible compared with the collinear direction of the propagating sound wave. The photoelastic constant P_{12} depends on three terms: (I) (Lorentz – Lorenz effect (LLE)); changes of the index of refraction due to sample's density described by a light induced strain; (II) (lattice effect (LE)); anisotropic correction of the index of refraction as a result of the elliptical distortion of the Lorentz cavity is caused by the light induced strain

resulted in the deformation of the lattice with no changes at the individual atomic sites, (III) (atomic effect (AE)); correlation term, reflecting an additional polarizing effect of neighboring atoms on each other causing the deformation of an individual atomic sites with no changes in the lattice.

The measured photoelastic constants P_{12} and P_{44} in the light of Carleton & Matusita theory are important parameters, so we can calculate polarizability α and correlation integral G from two linear equation (2.19) and equation (2.20). Polarizability is the relative tendency of the electron cloud of an atom to be distorted from its normal shape by the presence of a nearby ion or dipole that is, by an external electric field. The correlation integral is the probability that two points are within a certain distance from one another.

The polarizability and correlation integral G using measured values of P_{12} and P_{44} are as follows:

$$\alpha = \frac{M}{[4\pi\rho N_A] \left[\frac{n^4}{(n^2-1)^2} \left(P_{12} - \frac{8}{3} P_{44} \right) + \frac{2}{3} \right]} \quad (2.22)$$

$$G = \left[\frac{4\pi\rho N_A}{3M} \right] \left[1 - \frac{5n^4 P_{44}}{(n^2-1)^2} \right] \left[\frac{n^4}{(n^2-1)^2} \left(P_{12} - \frac{8}{3} P_{44} \right) + \frac{2}{3} \right] \quad (2.23)$$

where the index of refraction n , density ρ , and the calculated glass molar mass M are based on the glass composition.

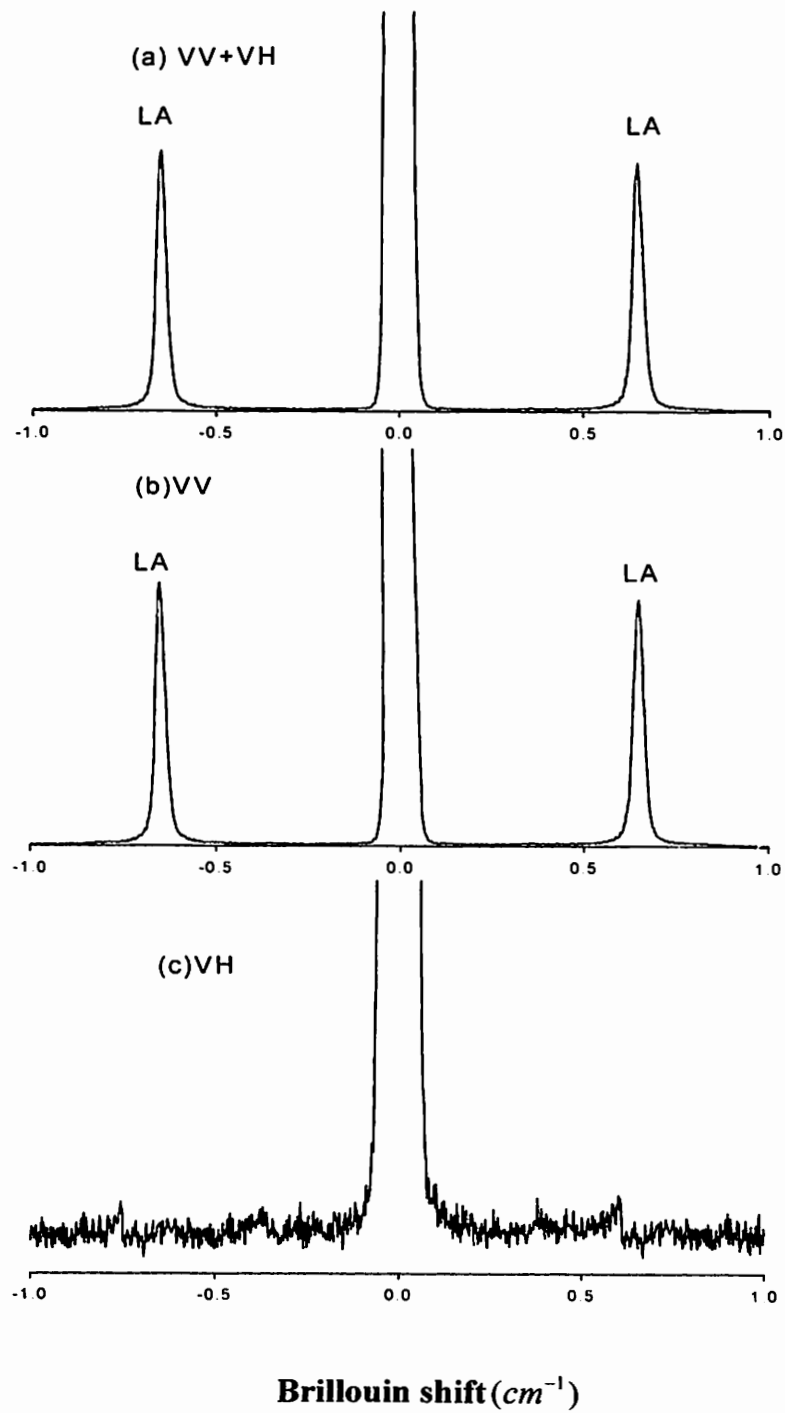


Fig. 3. Polarized BLS spectra of PbO.0.46 glass: (a) Vertical-Vertical+Vertical Horizontal (or VV+VH); (b) Vertical-Vertical (VV); (c) Vertical-Horizontal (VH)

Absorption coefficient measurement (see Fig 4):

$$I_T = I_0 \exp(-\alpha_{\text{absorption}} d)$$

$$\alpha_{\text{absorption}} = \frac{\ln\left(\frac{I_0}{I_T}\right)}{d} \quad (2.24)$$

where d is the thickness, $\alpha_{\text{absorption}}$ is the absorption coefficient of the sample at 514.5 nm

and I_0 is the initial light intensity and I_T is the transmission light intensity

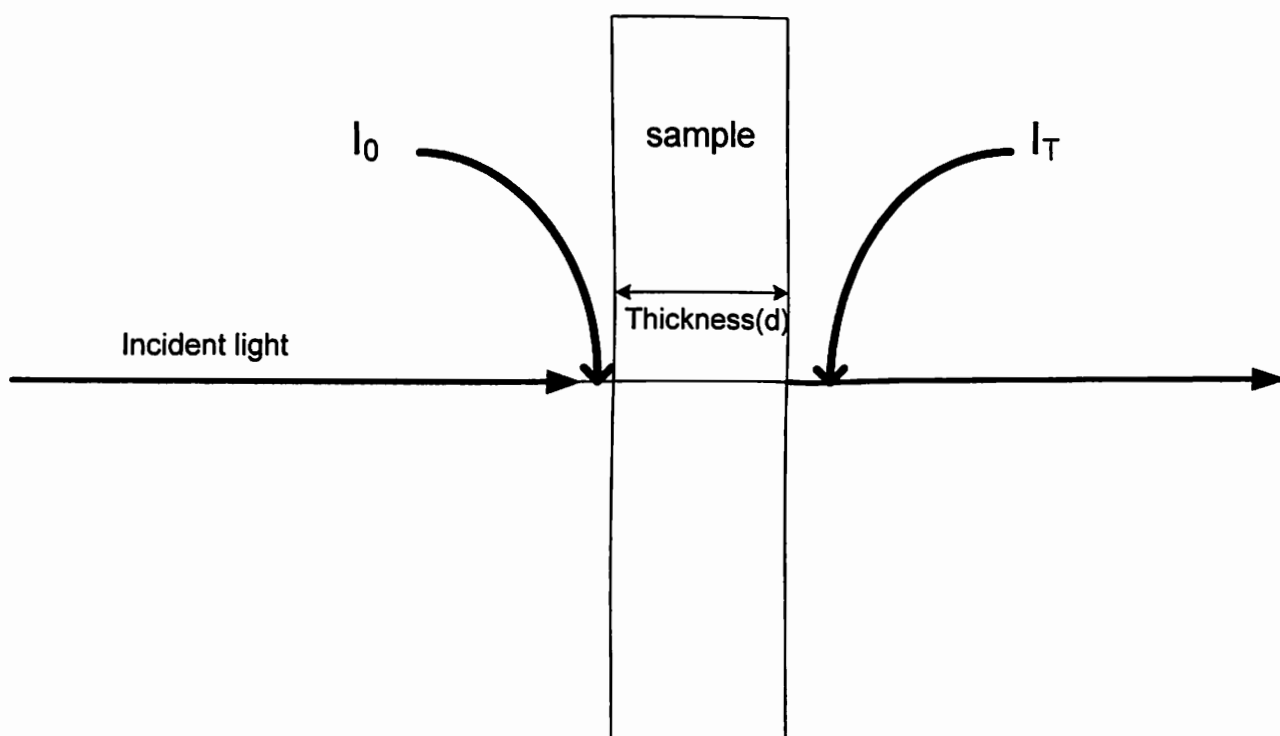


Fig . 4. The absorption measurement

Chapter III

Experiments

Samples preparation

A total of six glass samples were prepared with different weight percents of lead. All glasses were heated in platinum crucibles using chemicals from Aldrich Chemical Company, Inc with 99.9% purity. All glasses were allowed to form in the crucibles and then annealed at 20 °C lower than their respective glass transition temperatures. All samples were then polished using the Ecomet 3 (BUEHLER) grinder-polisher and cerium oxide.

1) $\text{XPbO} \cdot (0.62 - \text{X}) \cdot \text{Bi}_2\text{O}_3 \cdot 0.3\text{Ga}_2\text{O}_3 \cdot 0.08\text{B}_2\text{O}_3$; $\text{X} = 0$, this sample was heated at 1500 °C for 15 minutes before and after checking weight loss and annealed at 410 °C for 2 hours.

Dark regions caused by different cooling rates in the glass body are faintly visible.

2) $\text{XPbO} \cdot (0.62 - \text{X}) \cdot \text{Bi}_2\text{O}_3 \cdot 0.3\text{Ga}_2\text{O}_3 \cdot 0.08\text{B}_2\text{O}_3$; $\text{X} = 0.16$, this sample was heated at 1500 °C for 15 minutes before and after checking weight loss and annealed at 375 °C for 2 hours. Dark regions caused by different cooling rates in the glass body are faintly visible.

3) $\text{XPbO} \cdot (0.62 - \text{X}) \cdot \text{Bi}_2\text{O}_3 \cdot 0.3\text{Ga}_2\text{O}_3 \cdot 0.08\text{B}_2\text{O}_3$; $\text{X} = 0.31$, this sample was heated at 1500 °C for 15 minutes before and after checking weight loss and annealed at 410 °C for 2 hours. Dark regions caused by different cooling rates in the glass body are faintly visible.

- 4) $\text{XPbO} \cdot (0.62-X) \cdot \text{Bi}_2\text{O}_3 \cdot 0.3\text{Ga}_2\text{O}_3 \cdot 0.08\text{B}_2\text{O}_3$; $X= 0.46$, this sample was heated at 1500°C for 15 minutes before and after checking weight loss and annealed at 410°C for 2 hours. There are no dark regions visible.
- 5) $\text{XPbO} \cdot (0.62-X) \cdot \text{Bi}_2\text{O}_3 \cdot 0.3\text{Ga}_2\text{O}_3 \cdot 0.08\text{B}_2\text{O}_3$; $X= 0.62$, this sample was heated at 1500°C for 15 minutes before and after checking weight loss and annealed at 410°C for 2 hours. There are no dark regions visible.
- 6) $\text{XPbO} \cdot (0.7-X) \cdot \text{Bi}_2\text{O}_3 \cdot 0.3\text{Ga}_2\text{O}_3$; $X= 70$, this sample was heated at 1000°C for 10 minutes and was heated again at 410°C for 2 hours. The sample annealed at 410°C for 2 hours. There are no dark regions visible.

BLS experiment and procedures

Our goal is that we find the elastic and photoelastic properties of the lead bismuth gallate boron glasses. The BLS setup is shown in Fig.5. The light source is argon ion laser (Spectra Physics 2020) operating at 514.5 nm wavelength in a single TEM_{00} mode. The scattered light from sample is analyzed using 6-pass tandem Fabry-Perot interferometer (TFPI) with high contrast and finesse at room temperature (23°C) [18, 19]. The intensity of the scattered light is measured with a photomultiplier tube (Hamamatsu R-463) and recorded on a 1024-channel multi-channel analyzer (Canberra, 35 plus). The spectra then are downloaded to a PC. The signal is split for stabilization and monitoring using a spectrum digital to analog converter and an interferometer control unit. The output spectrum from the control unit is monitored on an oscilloscope (Soltec 520) in real time. The control unit also provides the trigger for the multichannel analyzer and also provides the signal to the shutter unit which

controlled the light modulator. The polarization rotator mounted to the laser head ensures the direction of the incident polarization is vertical (V) while the Brillouin scattered light entering the TFPI is polarized using a polarization analyzer. We can obtain two pair of peaks corresponding to the LA and TA acoustic modes by acquiring spectra having VV and VH polarization components, respectively.

The FP alignment is very complicated and important. We have to do the alignment of the 6-pass tandem Fabry-Perot interferometer (TFPI) before each experiment [see Fig.6 and Fig.7] We measure the Brillouin spectrum of a standard material (Plexiglas) prior to our sample measurement. The intensity of the obtained Brillouin longitudinal peak is usually over 40,000 counts/sec. The spectrum consists of a central Rayleigh peak and the two Brillouin peaks. The mirror gap of the first interferometer is set at 2.5 or 2.75 mm giving a free spectral range of 2 or 1.818 cm^{-1} . The contrast of the system is about 10^9 , and the overall finesse is about 120. The dwell time is set for 0.5 ms/ch, and each FP scan lasts 0.5 seconds. Each data file contained 1024 channels (histogram) and took anywhere from 30 to 60 minutes to collect. The Brillouin scattered light was collected at right angle ($\theta = 90^\circ$) with respect to the direction of the incident light. The most accurate method of measuring elastic constants is based on the use of ultrasonic sound velocity measured by the Brillouin scattering experiment [20].

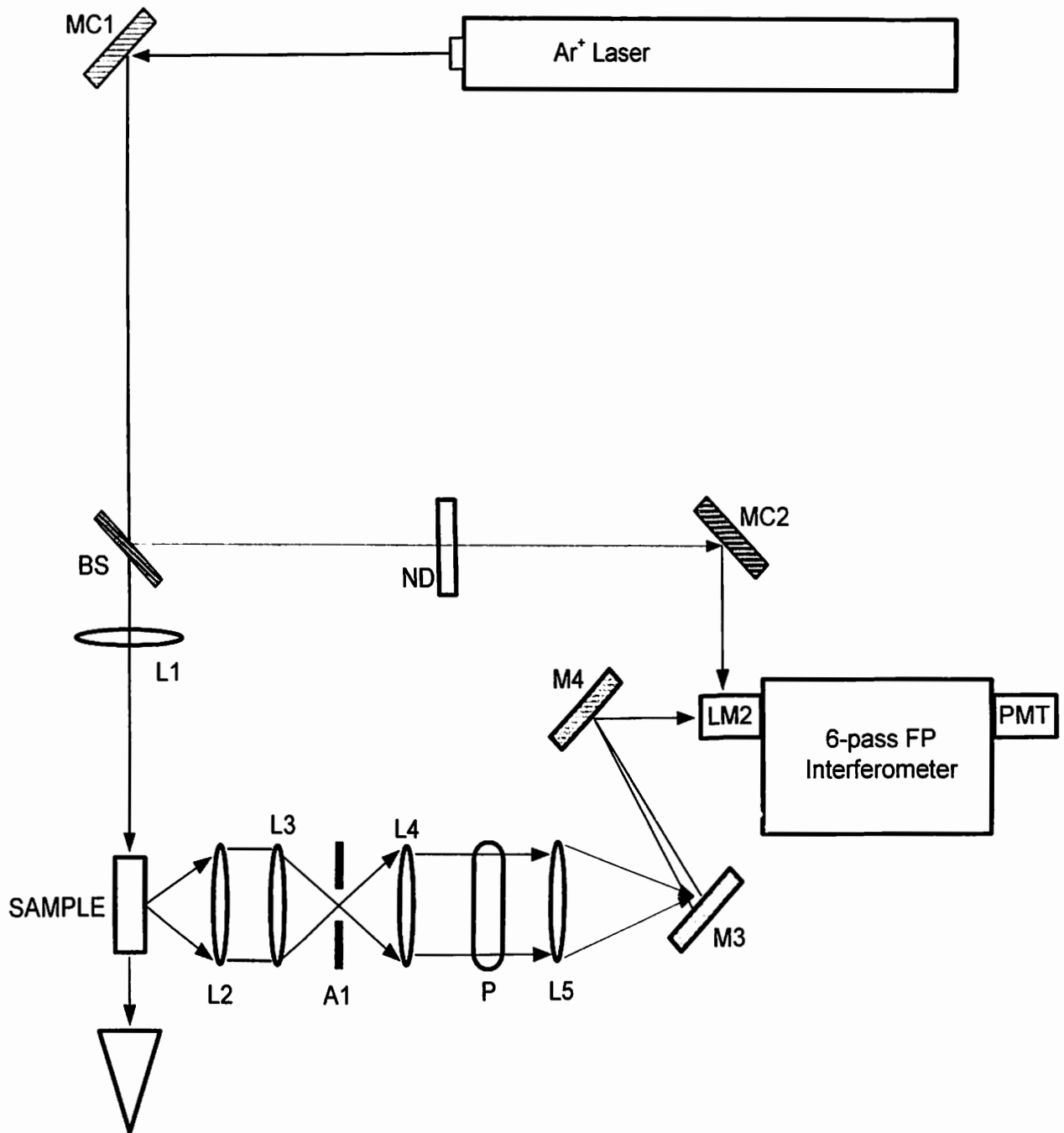


Fig. 5. 6-pass tandem Fabry-Perot interferometer

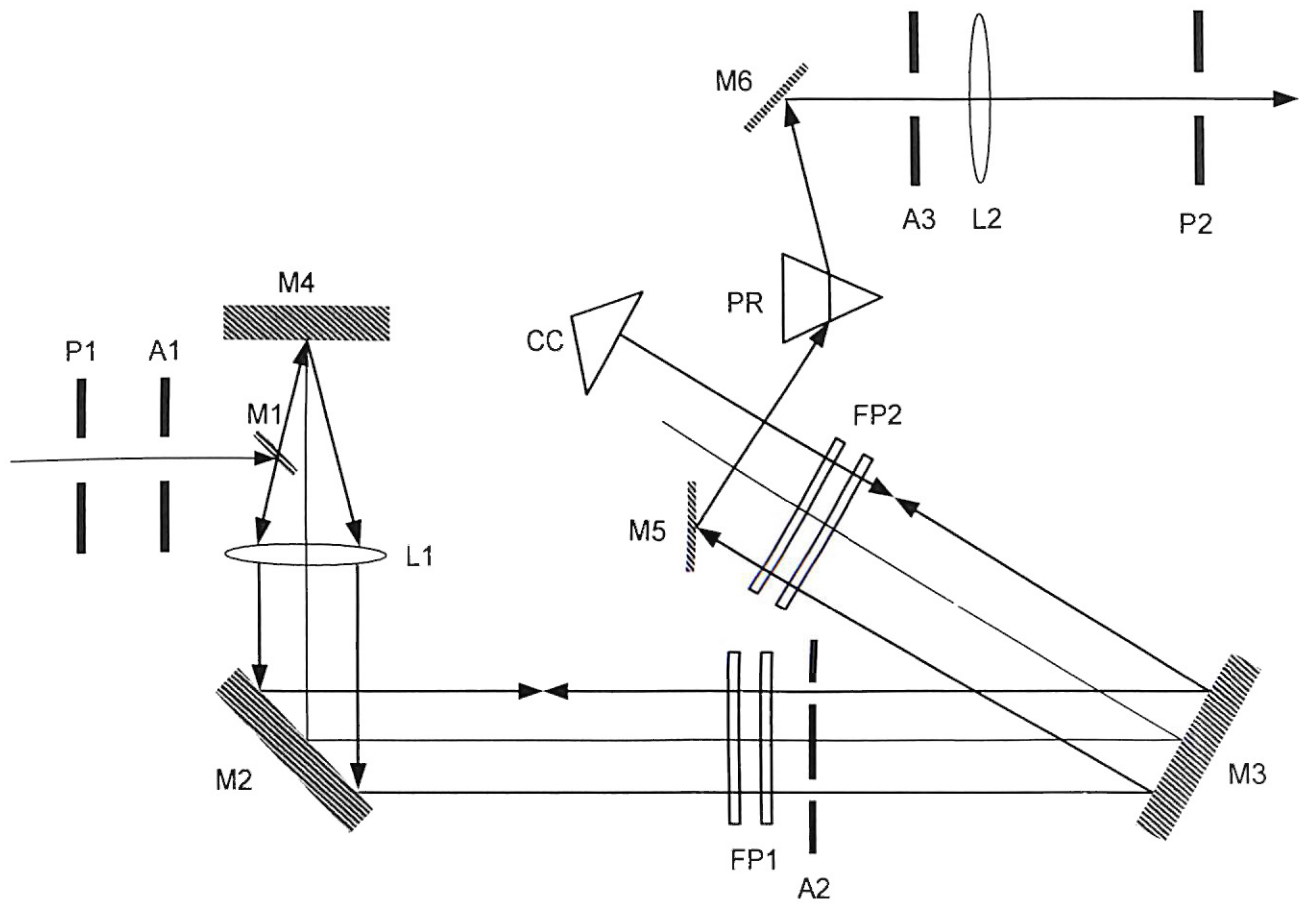


Fig. 6. Optics and optical path ways within 6-pass tandem Fabry-Perot interferometer.

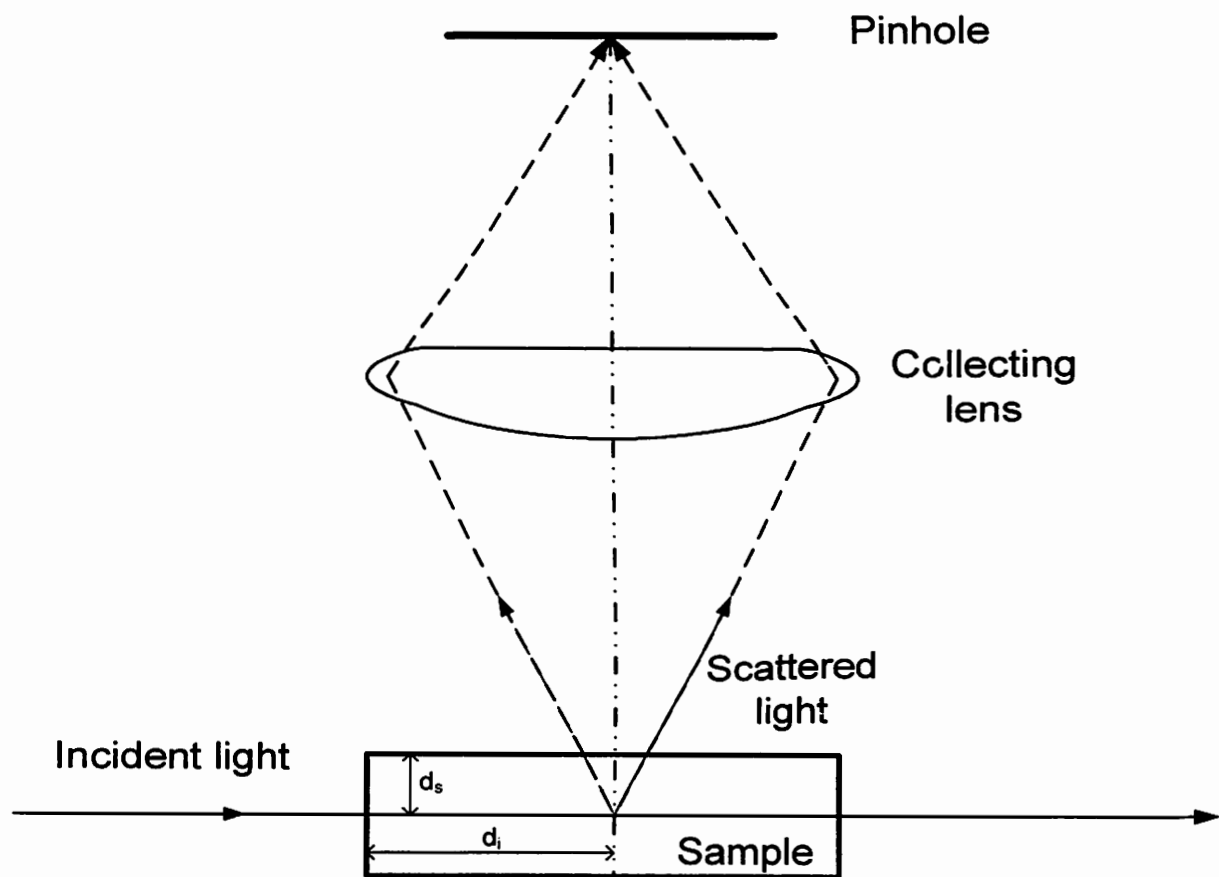


Fig . 7. Top view of the sample for the incident and scattered light distance.

Refractive Index Measurements using a CCD

We measure the refractive index of materials using an enhanced version of the Brewster's angle experiment. This experiment is usually used to estimate of the refractive index to about one or two decimal places. This technique needs one polished surface and can be applied to both transparent and opaque materials. At the Brewster's angle, only s-polarized light is reflected [21]. If the reflected intensity reaches a minimum, then the reflected intensity for p-polarized light has been minimized indicating that the angle of reflection equals the Brewster's angle.

We measure the Brewster's angle by monitoring the intensity change using a CCD camera. We have found that by introducing a CCD camera with a laser beam profiler to monitor the intensity change, we can isolate the angle close to the resolution of the sample rotation stage. We can easily find the refractive index from the relation $n = \tan \theta_B$. The refractive index measurement experimental setup is as shown in Fig. 8.

This experimental setup can simply be assembled and requires the sample, laser source, a sample holder, rotation stage, CCD camera, a laser beam profiler, and neutral density filters. The most important thing is that the incident laser beam is perpendicular to the sample surface. This can be easily achieved by aligning the back-reflected beam. For more accurate measurements, we place a pinhole at the center of the incident laser beam and close to the laser source. The back reflected diffraction rings are properly centered on the pinhole.

We now slowly rotate the sample and place a card about 10 to 20 cm from the reflected beam and check the change in the reflected intensity by eye. When

we find a very weak reflected intensity, we move the CCD camera in place. By making small rotational increments, we can watch the minimum intensity on the monitor of the laser beam profiler as we rotate through the Brewster's angle. We can determine the angle close to the resolution of our rotation stage (0.01°). We can easily scan through the Brewster's angle without having to adjust the camera position. To prove the accuracy of this technique, we measured the refractive index of a fused quartz sample [22]. At the incident laser wavelength 514.5 nm, the Brewster's angle is $55.63^\circ \pm 0.05^\circ$ so a refractive index is 1.462 ± 0.003 . The uncertainty reported is larger than that of the minimum-deviation technique because we found it hard to accurately isolate the Brewster's angle to any better than $\pm 0.05^\circ$ as a result of laser fluctuations. The reason for this is that the monitored reflected intensity change is the determining criteria for the Brewster's angle.

Density Measurements

We measured the density of each glass sample using Archimedes's method with an error of less than $\pm 0.89\%$. The samples were immersed into distilled water, the density of which is very well known. The density was determined as the ratio of the glass sample mass to the volume of the displaced distilled water.

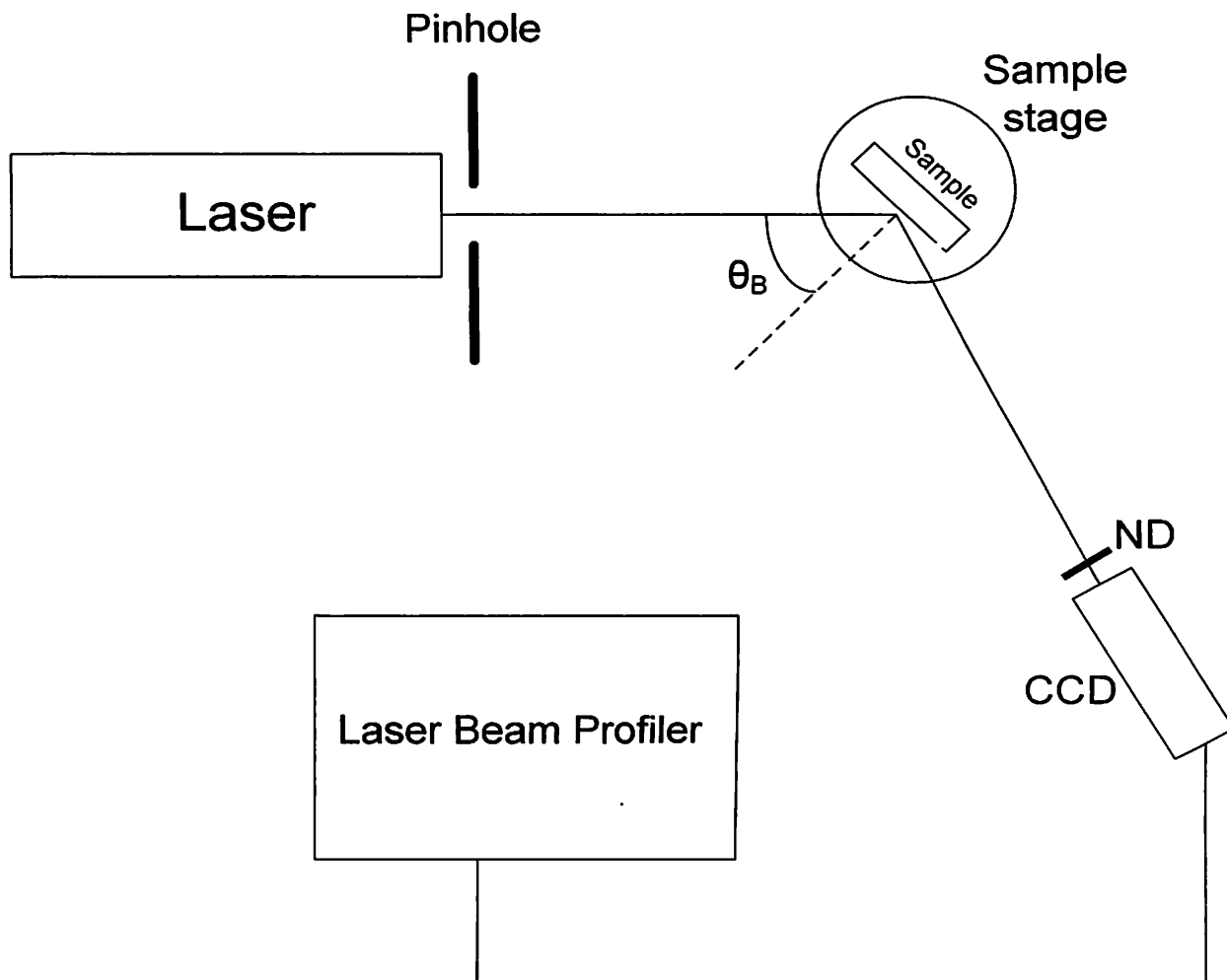


Fig. 8. Setup for Refractive Index Measurements

Chapter IV

RESULTS AND DISCUSSION

Results

Brillouin shifts (ω_L)

The Brillouin spectra for the lead bismuth gallate boron glasses in right angle scattering geometry are shown in Fig.9. We could not find a transverse Brillouin shift (ω_T).

The results of longitudinal Brillouin shifts (ω_L) measurements are shown in Table 3.

Sample ID	Density ρ (g/cm^3)	ω_L (cm^{-1})	Index of refraction (at 514.5nm)
PbO.0 Bi₂O₃.0.62	7.003 ± 0.011	0.715 ± 0.019	2.340 ± 0.010
PbO.0.16 Bi₂O₃.0.46	6.503 ± 0.025	0.680 ± 0.003	2.305 ± 0.005
PbO.0.31 Bi₂O₃.0.31	6.900 ± 0.011	0.668 ± 0.053	2.290 ± 0.009
PbO.0.46 Bi₂O₃.0.16	6.619 ± 0.059	0.681 ± 0.005	2.255 ± 0.009
PbO0.62 Bi₂O₃.0	6.100 ± 0.014	0.657 ± 0.009	1.679 ± 0.009
PbO0.70 Bi₂O₃.0	7.020 ± 0.048	0.646 ± 0.001	1.617 ± 0.008
Fused silica	2.21	0.794	1.462

Table 3. Brillouin shifts (ω_L), refractive indices n , and density ρ

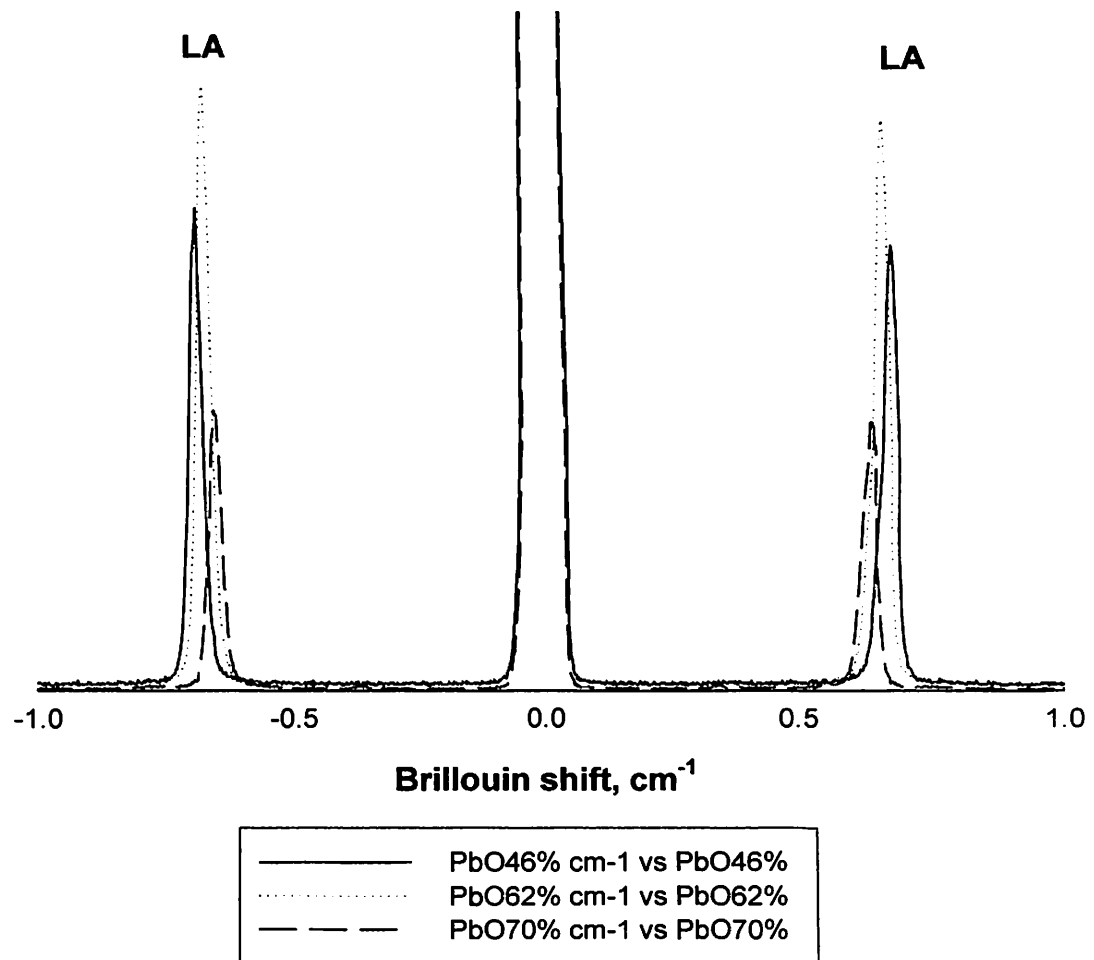


Fig. 9. Brillouin spectra of lead bismuth gallate boron glasses (our measurements)

The sound velocities (the acoustic phonon velocities) of our samples were calculated from the Brillouin shifts (ω_L) using equation (2.4).

Elastic parameters

An elastic constant is related with the Brillouin shifts (ω_L), refractive indices n , and density ρ . However, we could not determine the elastic constant (C_{44}) for the TA Phonon since these were not addressed in this study. The results of BLS measurements are shown in Table 4. Using equation (2.12), we can calculate the elastic constants (C_{11}). These are shown in Table 4 and a plotted in Fig. 10.

Sample ID	v_{LA} (10^5 cm/s)	C_{11} ($10^{11} \text{ dynes/cm}^2$)
PbO.0 Bi₂O₃.0.62	3.330 ± 0.085	7.768 ± 0.044
PbO.0.16 Bi₂O₃.0.46	3.220 ± 0.014	6.742 ± 0.059
PbO.0.31 Bi₂O₃.0.31	3.180 ± 0.028	6.978 ± 0.012
PbO.0.46 Bi₂O₃.0.16	3.310 ± 0.014	7.190 ± 0.099
PbO0.62 Bi₂O₃.0	4.274 ± 0.065	11.140 ± 0.003
PbO0.70 Bi₂O₃.0	4.360 ± 0.007	13.34 ± 0.001

Table 4. Sound velocities and calculated elastic constants C_{11} vs PbO mole%

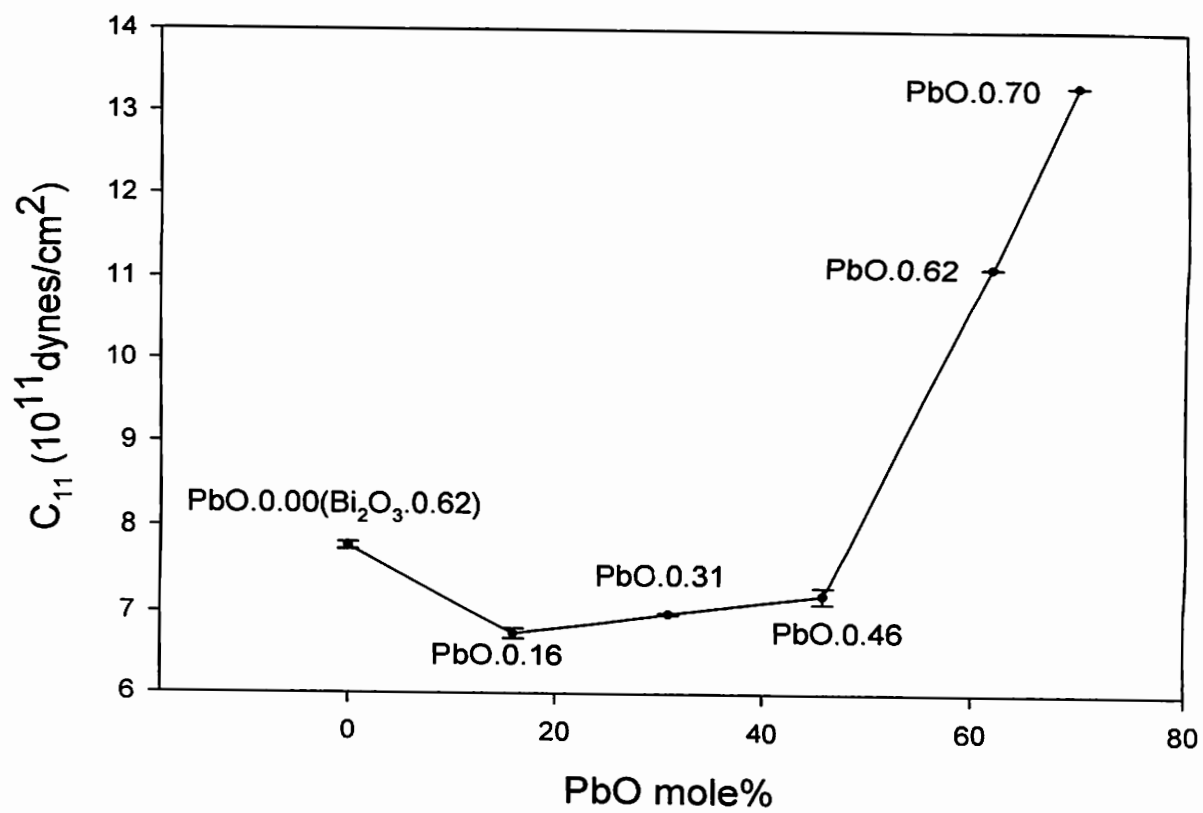


Fig. 10. Calculated elastic constants (C_{11}) vs. PbO mole %

Photoelastic constants

We calculate the photoelastic constants (P_{12}) which correspond to longitudinal acoustic mode using equation (2.18). Once again, we cannot calculate photoelastic constants (P_{44}) which correspond to transverse acoustic mode. Measurements of the photoelastic constants (P_{12}) were only obtained from glass samples with smaller light absorptions (PbO.0.46, PbO.0.62, and PbO.0.70). The values of the photoelastic constants (P_{12}) are given in Table 5 and plotted for these samples in Fig. 11.

Sample ID	P_{12}
PbO.0.46 Bi ₂ O ₃ .0.16	0.093 ± 0.086
PbO0.62 Bi ₂ O ₃ .0	0.279 ± 0.041
PbO0.70 Bi ₂ O ₃ .0	0.278 ± 0.078

Table 5. Photoelastic constants (P_{12}) vs. PbO mole%

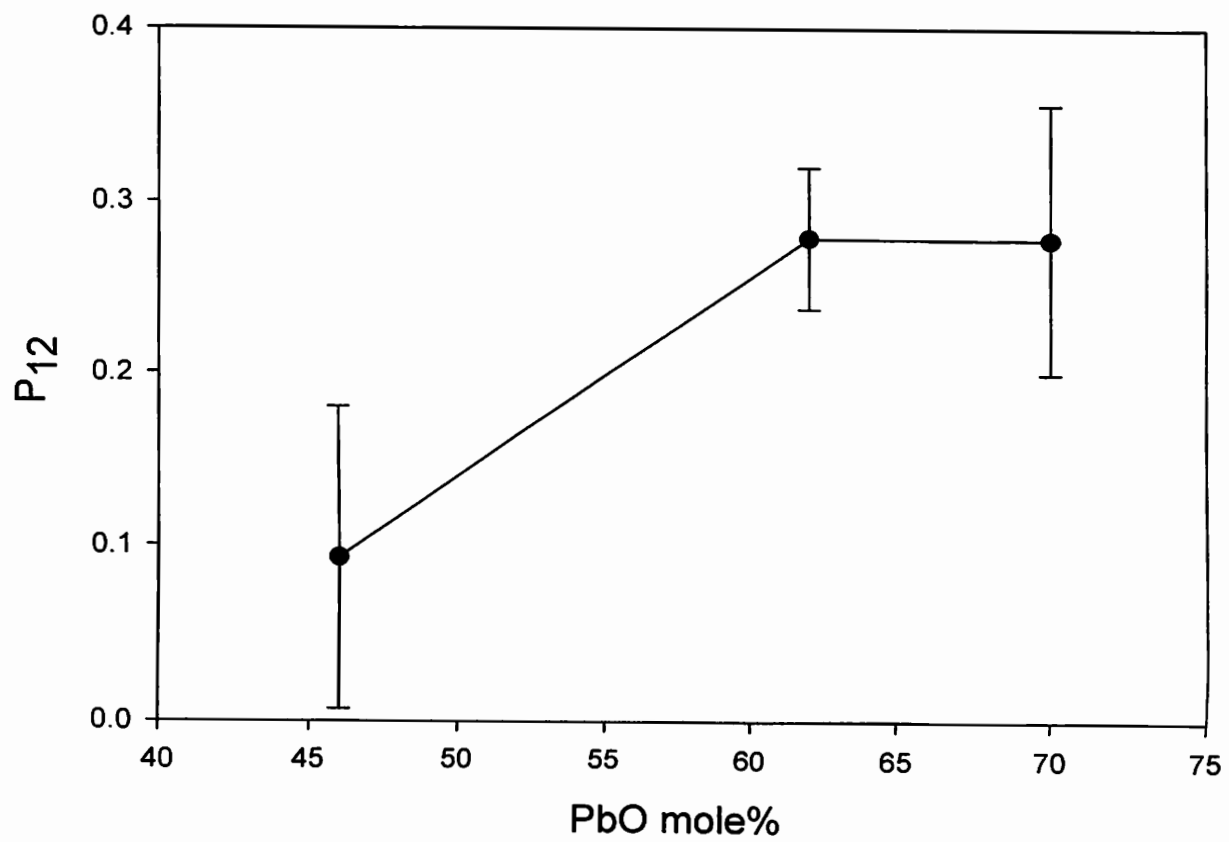


Fig. 11. Calculated photoelastic constants (P_{12}) vs. PbO mole %

Lorentz – Lorenz effect (LLE), Lattice effect (LE), Atomic effect (AE)

We have calculated the expected contributions of *LLE*, *LE*, and *AE* to the photoelastic constants (P_{12}) using equations (2.19), (2.20) according to the suggestion of Carleton [15] and Matusita [16]. The results of these calculations are shown in Table 6 and plotted in Fig.12, Fig. 13, and Fig. 14.

Sample ID	LLE	LE	AE
PbO.0.46	0.523 ± 0.002	$-(0.069 \pm 0.001)$	$-(0.279 \pm 0.001)$
PbO.0.62	0.553 ± 0.006	$-(0.056 \pm 0.001)$	$-(0.223 \pm 0.002)$
PbO.0.70	0.506 ± 0.007	$-(0.050 \pm 0.001)$	$-(0.214 \pm 0.003)$

Table 6. Lorentz – Lorenz effect (LLE), Lattice effect (LE), Atomic effect (AE) contributions to the photoelastic constants (P_{12}).

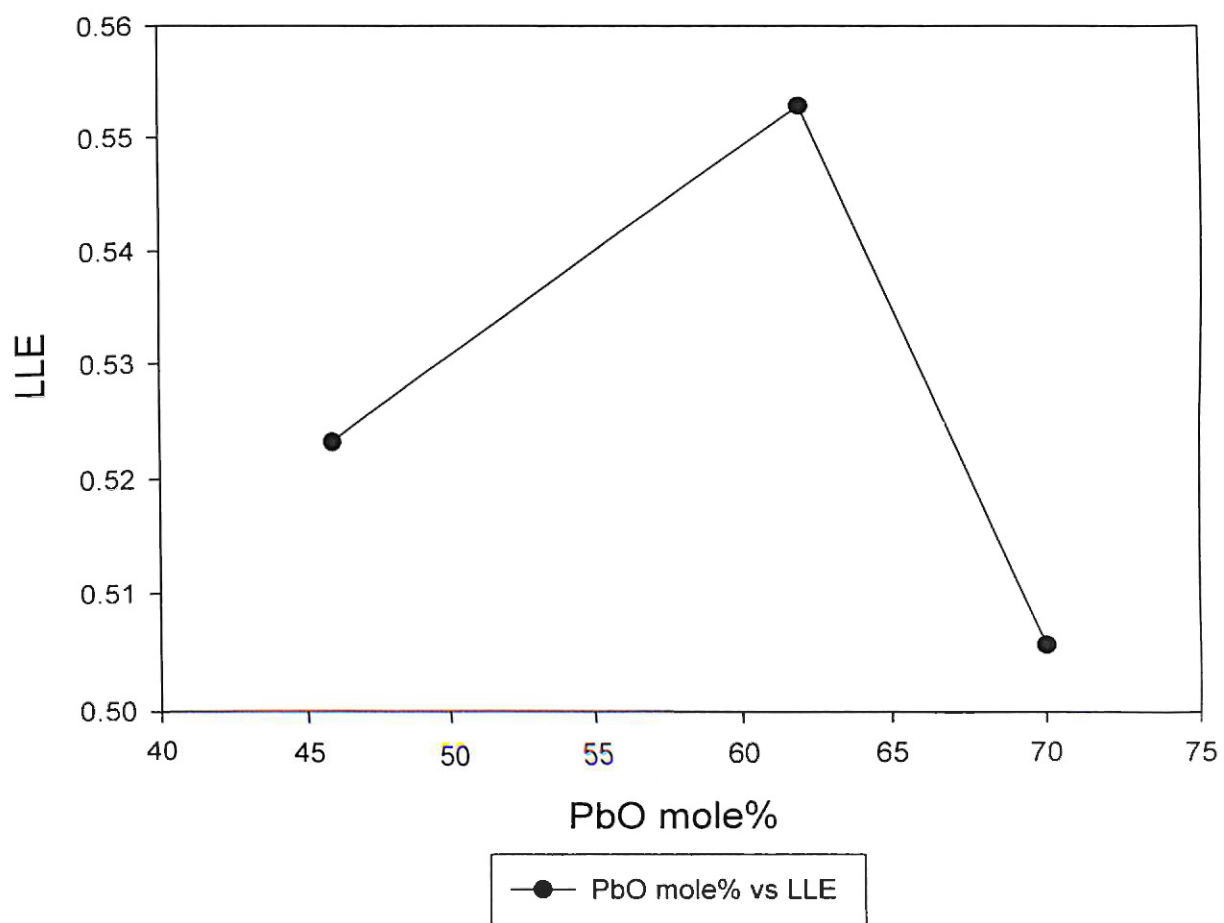


Fig. 12. Lorentz – Lorenz effect (LLE) vs. PbO mole %

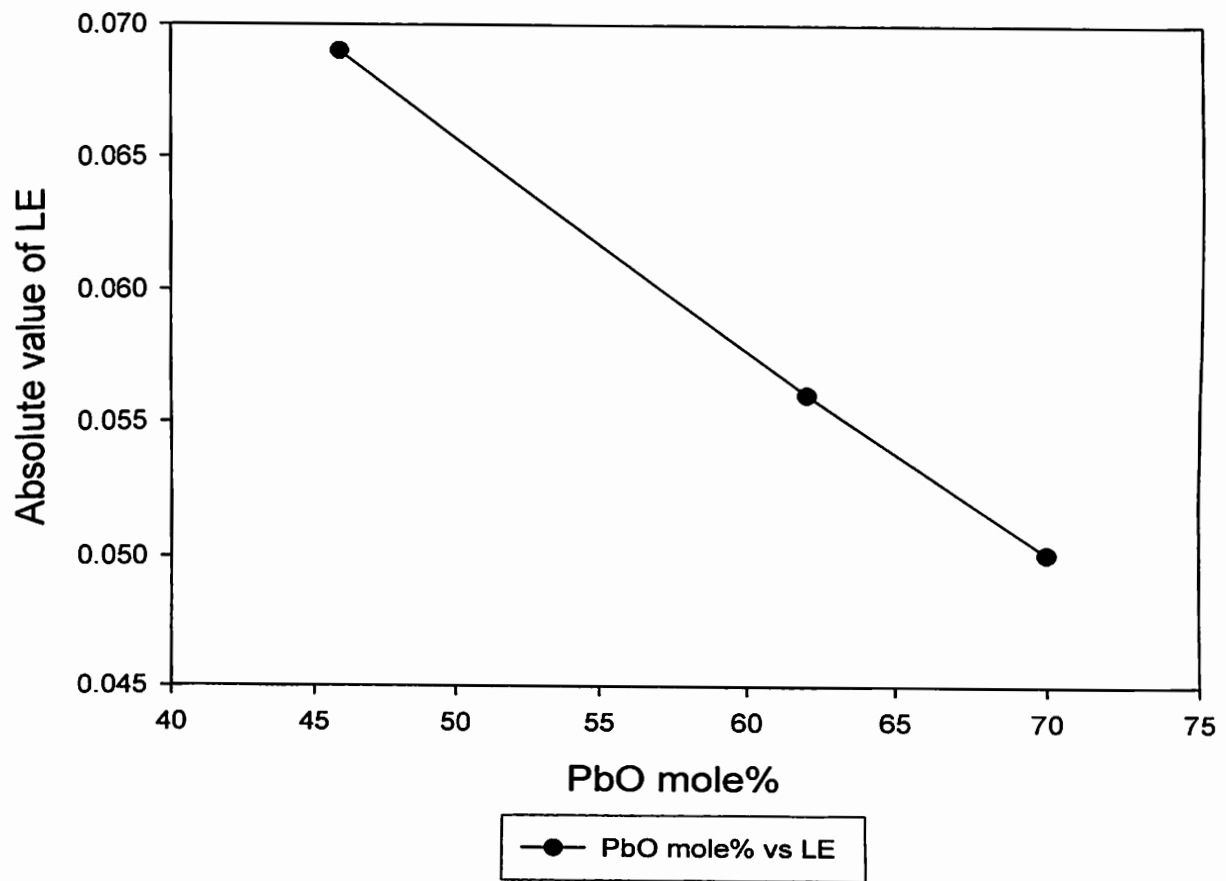


Fig. 13. Lattice effect (LE) vs. PbO mole %

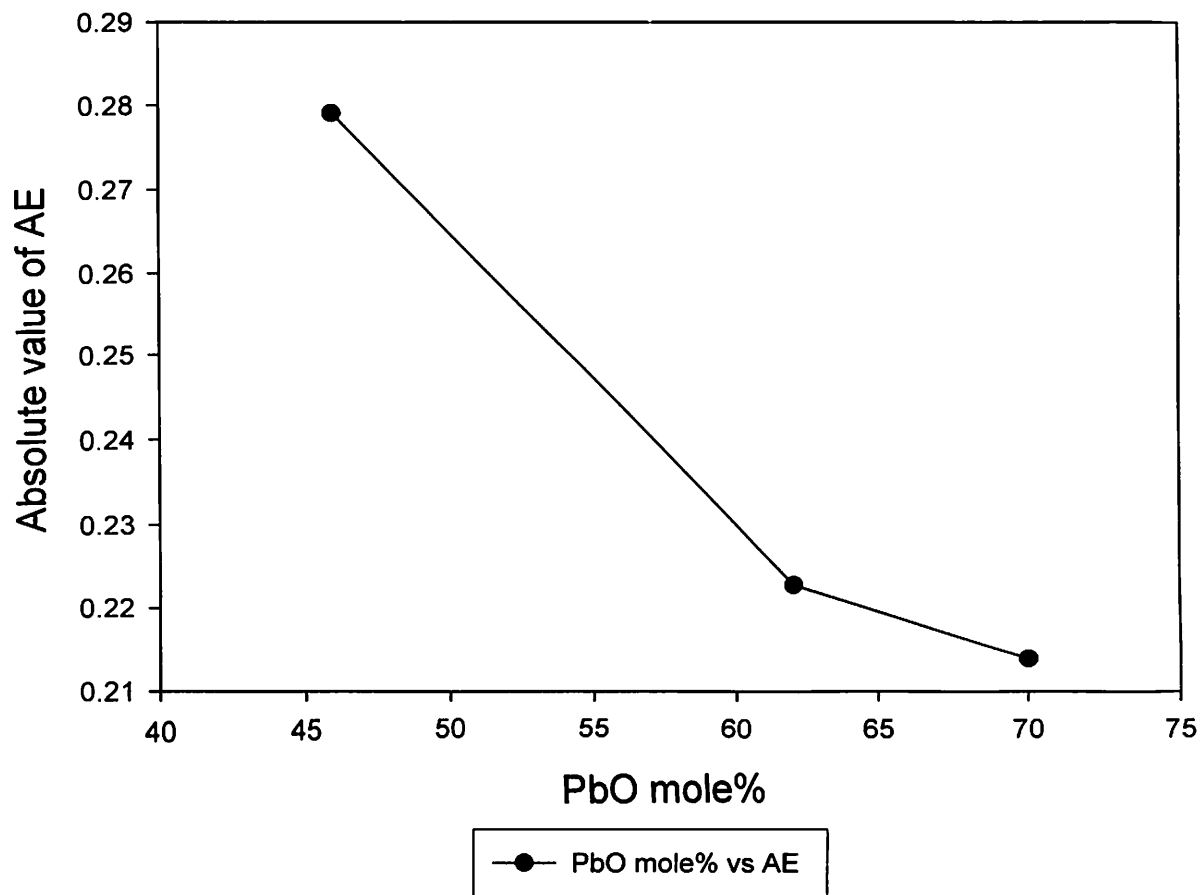


Fig. 14. Atomic effect (AE) vs. PbO mole %

Polarizability α

We calculated the polarizability (α) using equation (2.22). This value is based on molar mass M , P_{12} , P_{44} , n , ρ and Avogadro's number. Here, we assumed that P_{44} is zero. The results of the polarizabilities (α) are shown in Table 7 and plotted in Fig. 14.

Sample ID	PbO (mole%)	Bi₂O₃ (mole%)	Ga₂O₃ (mole%)	B₂O₃ (mole%)	M (g/mol)	Polarizability α (10⁻²³cm³)
PbO.0.46	46	16	30	8	229.426	0.565 ± 0.019
PbO.0.62	62	0	30	8	210.585	0.343 ± 0.025
PbO.0.70	70	0	30	0	202.871	0.288 ± 0.030

Table 7. Polarizability α

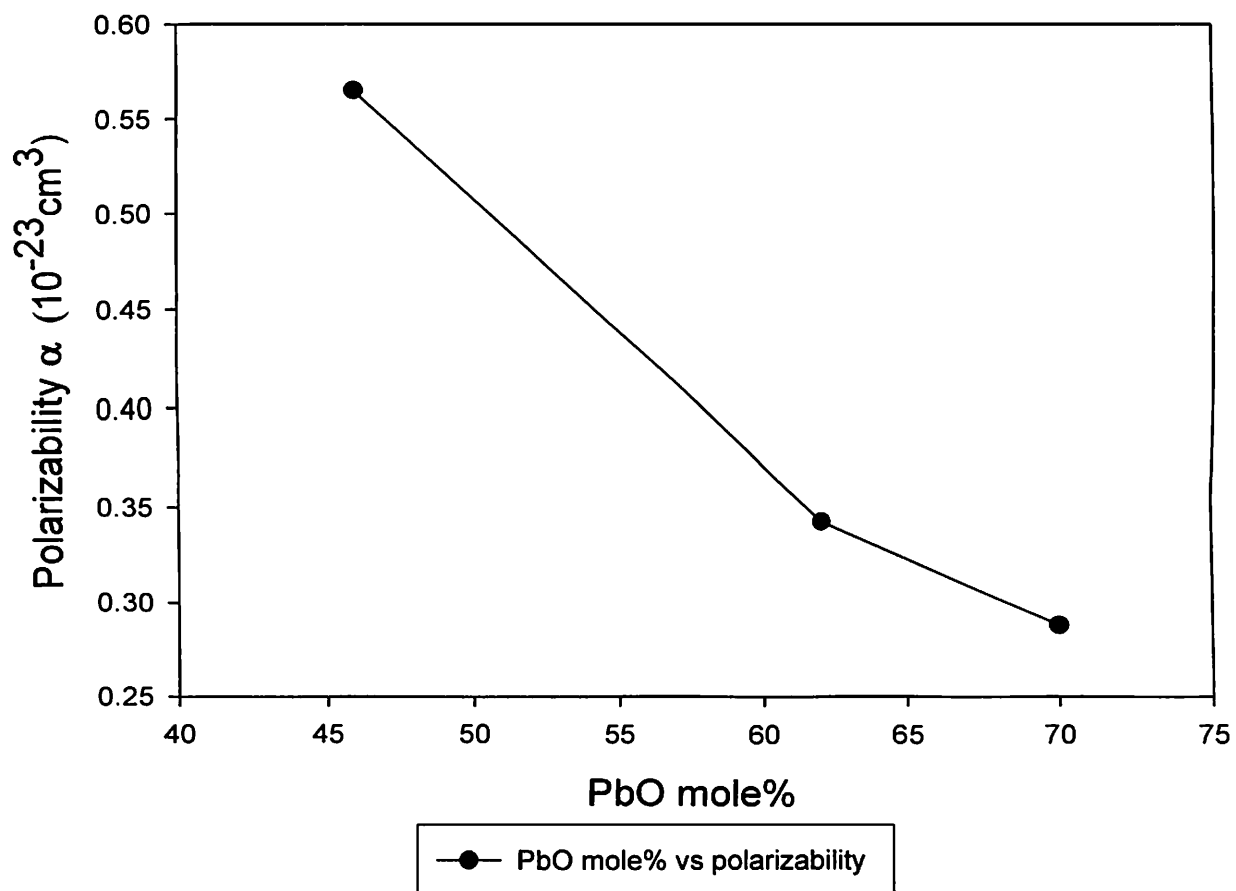


Fig. 14. Polarizability α vs. PbO mole %

Correlation integral G

We have calculated the correlation integral G using equation (2.23). This is based on the molar mass M , P_{12} , P_{44} , n , ρ , and *Avogadro's number*. Here, we assumed that P_{44} is zero. The results of the correlation integrals (G) are shown in Table 8. and plotted in Fig. 16.

Sample ID	PbO (mole%)	Bi ₂ O ₃ (mole%)	Ga ₂ O ₃ (mole%)	B ₂ O ₃ (mole%)	M (g/mol)	G (10 ²³ cm ³)
PbO.0.46	46	16	30	8	229.426	0.590 ± 0.019
PbO.0.62	62	0	30	8	210.585	0.976 ± 0.072
PbO.0.70	70	0	30	0	202.871	1.219 ± 0.178

Table 8. The correlation integral G

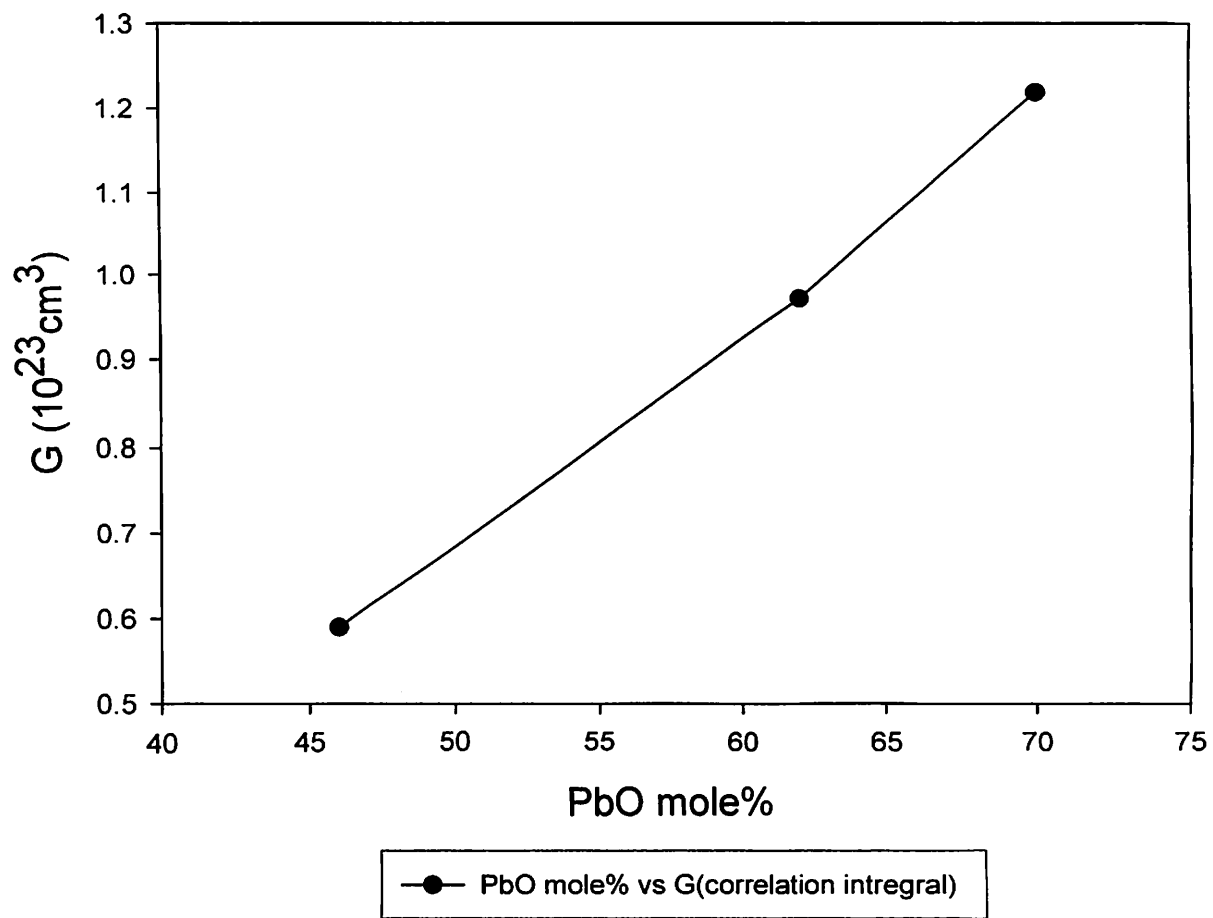


Fig. 16. The correlation integral G vs. PbO mole %

Absorption coefficients

We calculated absorption coefficients ($\alpha_{\text{absorption}}$) using equation (2.24) for intensity I_T . The results of absorption coefficients ($\alpha_{\text{absorption}}$) are shown in Table 9 and plotted in Fig. 16.

Sample ID	Absorption $\alpha_{\text{absorption}} (\text{cm}^{-1})$	Absorption (using Cary 05) $\alpha_{\text{absorption}} (\text{cm}^{-1})$
PbO.0.46	0.241 ± 0.001	0.232
PbO.0.62	0.384 ± 0.001	0.332
PbO.0.70	0.848 ± 0.001	0.908

Table 9. Absorption coefficients ($\alpha_{\text{absorption}}$)

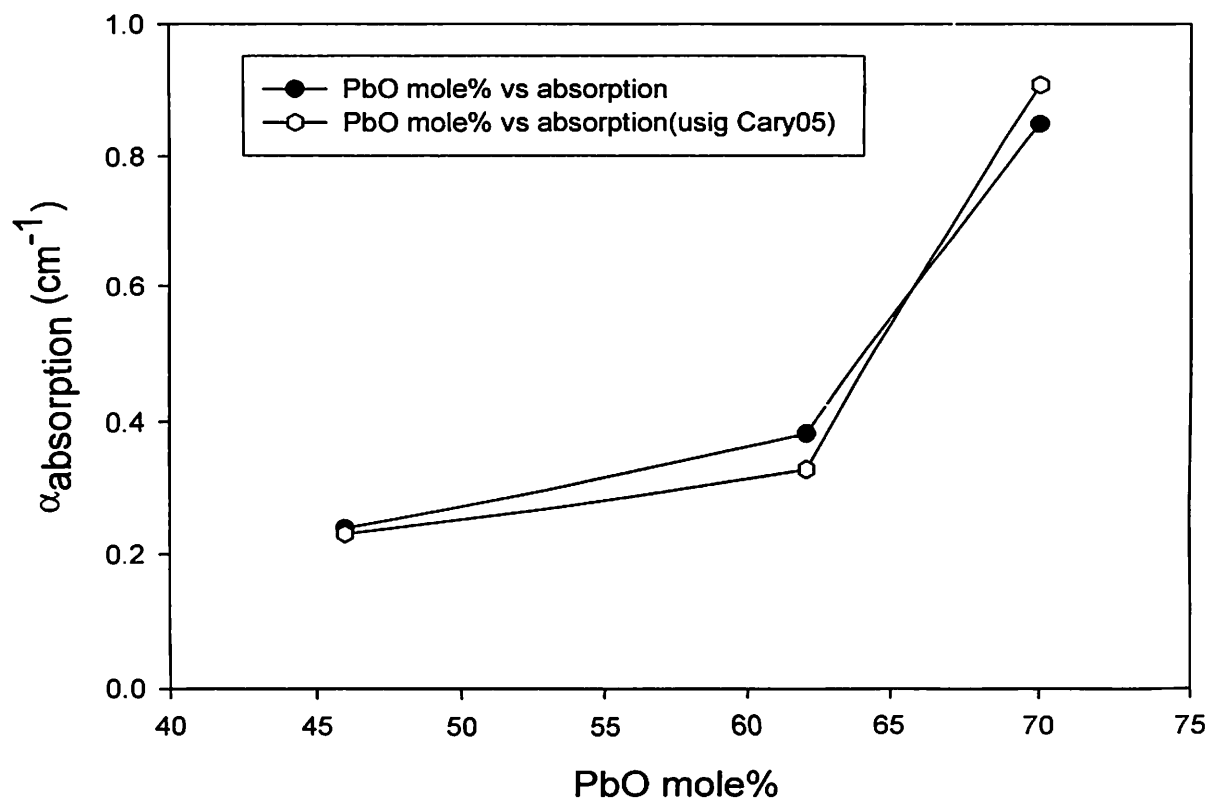


Fig. 17. Absorption coefficients ($\alpha_{\text{absorption}}$) vs. PbO mole %

By analyzing Fig. 9, we note that these glass samples have very small transverse acoustic Brillouin modes and thus, transverse acoustic Brillouin modes are hard to obtain. It is assumed that most Pb^{2+} and Bi^{3+} ions in these glass samples are considered to act as network formers [23]. Ga_2O_3 is a modifier. It is known that Ga_2O_3 alone does not form glasses, while binary gallate systems containing alkali, alkaline earth oxide and lead oxide form glasses [24]. The possible coordination numbers of Pb^{2+} are between 6 and 8. The possible coordination numbers of Bi^{3+} are between 6 and 8. The coordination number of silicon silicate glasses is 4 [1]. These results of very small transverse acoustic Brillouin modes have been attributed to high coordination of the glass sample, especially when compared to silicate glasses [25]. A similar observation is demonstrated by Grishin et al., [25] where no transverse Brillouin components are reported from heavy metal fluoride glass samples.

The elastic constant (C_{11}) depends on bonding strength. As to the coordination of Pb^{2+} ions, Lveventhal and Bray [26] indicated from ^{207}Pb NMR measurements that most lead atoms act as network formers in $PbO-SiO_2$ glasses. The covalency of Pb-O bond increases with increasing PbO content at high PbO concentrations (Over 30% PbO) [5]. We can easily see from the last five samples (PbO.0.16, PbO.0.31, PbO.0.46, PbO.0.62, PbO.0.70), which include PbO, that a sample includes high PbO concentrations, it will have strong bonding. Thus the elastic constant (C_{11}) increases (see Table 4, Fig. 10).

We see that $|LE| < |AE| < LLE$, i.e. the largest contribution to P_{12} values come from Lorentz-Lorenz effect (LLE). Lorentz-Lorenz effect (LLE) (Fig.12) accounts for the change of refractive index due to local density changes accompanying the light induced strain. When we calculate LLE , it is proportional to the reciprocal of the polarizability

$\left(\frac{1}{\text{polarizability}} \right)$. At a small PbO content, the polarizability increases from the results (Table 7 and Fig. 14). If a sample includes high PbO concentrations, the covalency of Pb-O bond increases. This means their bonding is strong. Thus, electron cloud of an atom is hard to distort. Photoelastic constant (P_{12}) depends on the polarizability because of Lorentz-Lorenz effect (LLE). The Photoelastic constant (P_{12}) increases. In addition, the lattice effect is caused by the change of atomic position produced by the stress (Fig.13). If a sample includes high PbO concentrations, the covalency of Pb-O bond increases. The atomic position change is small so LE decreases. The atomic effect is caused by the deformation of electron clouds (Fig.14). When stress is applied to the glass, the bond angles forced to change and accordingly the electron clouds are distorted. If a sample includes high PbO concentrations, the covalency of Pb-O bond increases. Electrons are tightly bonded to the directional covalent bonds. Thus, AE decreases. The lattice effect (LE) is smaller than the atomic effect (AE) because it is easier to distort individual atomic sites than the group of atoms (lattice). The polarizability (α) values decrease in a similar manner as LE and AE. If a sample includes high PbO concentrations, the covalency of Pb-O bond increases. The correlation integral (G) is proportional to the presence of $\frac{1}{r^4}$. The bond length is short in the strong bond. Thus, the correlation integral linearly increases (Fig.16). If the glass samples contain more heavy metal concentration (Pb^{2+} or Bi^{3+}) the absorption coefficients increase.

Chapter V

Conclusion and Future work

This dissertation focused on the optical properties (elastic constant C_{11} and photoelastic constant P_{12}) of lead bismuth gallate boron glasses. We tried to understand these properties in terms of the composition changes that occurred among glass samples of family. By understanding the structure of the glass samples provides reasonable explanation of the optical properties.

The elastic constant (C_{11}) is influenced by bonding strength. Thus, the elastic constant (C_{11}) increases for samples with high PbO concentrations, since the covalency of Pb-O bond increases [26].

The observed photoelastic constants (P_{12}) were compared to Carleton & Matusita theoretical expressions and discussed in terms of such structural variations as the average polarizability, density, index of refraction, absorption coefficient, molar mass, Lorentz-Lorenz effect, lattice effect and atomic effect. The Lorentz-Lorenz effect was the dominant contribution to the photoelastic constant P_{12} . Lorentz-Lorenz effect (LLE) is proportional to the reciprocal of the polarizability $\left(\frac{1}{\text{polarizability}}\right)$. Thus, the photoelastic constant P_{12} depends on the polarizability. The lattice effect was found smaller than the atomic effect because it is easier to distort individual atomic sites than a group of atoms. The increase of the correlation integral (G) is related to the radial distribution which was attributed to the bond length. The study of the lead bismuth

gallate boron glasses show that very weak transverse acoustic phonons can be observed. The Photoelastic constants (P_{44}) are almost zero. This indicates that our samples have a more coordinated structure than silicate glass compounds [25].

For the past three decades, there has been significant fundamental interest in the optical responses of glasses. Optical studies in glasses are further complicated by the fact that most glasses are multi-component systems, where the components assume the role of network formers and network modifiers. The measurements of the photoelastic constants (P_{12}) were only obtained from glass samples with small light absorption (PbO0.46, PbO0.62, and PbO0.70). Higher quality glass samples are also needed to observe the TA modes. Clearly, there is a need for additional experimental work to elucidate the role of network formers and modifiers in the optical responses of glasses and, in general, to stimulate further theoretical studies in this area. Raman measurements are also needed to study optical phonon changes in glass samples with varying compositions.

BIBLIOGRAPHY

- [1] W. H. Dumbaugh, "Heavy metal oxide glasses containing Bi_2O_3 ," *Phys. Chem. Glasses* 27, 119-123 (1986).
- [2] D. W. Hall, M. A. Newhouse, N. F. Borrelli, W. H. Dumbaugh, and D. L. Weidman, "Nonlinear optical susceptibilities of high-index glasses," *Appl. Phys. Lett.*, 54, 1293 (1989).
- [3] H. Nasu, J. Matsuoka, and K. Kamiya, "Second- and third-order optical non-linearity of homogeneous glasses," *J. Non-Cryst. Solids*, 178, 23-30 (1994).
- [4] I. Kang, T. D. Krauss, F. W. Wise, B. G. Aitken, and N. F. Borrelli, "Femtosecond measurement of enhanced optical nonlinearities of sulfide glasses and heavy-metal-doped oxide glasses," *J. Opt. Soc. Am. B* 12, 2053-2059 (1995).
- [5] F. Miyaji and S. Sakka, "Structure of $\text{PbO-Bi}_2\text{O}_3\text{-Ga}_2\text{O}_3$ glasses," *J. Non-Cryst. Solids*, 134, 77-85 (1991).
- [6] S. M. Mian, A. Y. Hamad, and J. P. Wicksted, "Refractive index measurements using a CCD," *Appl. Opt.*, 35, 6825 (1996).

- [7] Z. Pan, S. H. Morgan, and B. H. Long, "Raman scattering cross-section and non-linear optical response of lead borate glasses," *J. Non-Cryst. Solids.*, 185, 127-134 (1995).
- [8] Miyaki, T. Yoko, J. Jin, S. Sakka. T. Fukunaga, M. Misawa, "Neutron and x-ray diffraction studies of PbO-Ga₂O₃ and Bi₂O₃-Ga₂O₃ glasses," *J. Non-Cryst. Solids*, 175, 211-223 (1994).
- [9] L. Brillouin, *Ann. Phys.*, 17, 88 (1922).
- [10] J.F. Nye, *Physical properties of Crystals*, (Clarendon, Oxford 1957).
- [11] H. R. Carleton, *Amorphous Materials*, eds. R. W. Douglas and Bryan Ellis (Wiley, Interscience, New York, p.103, (1972); *Bull. Am. Phys. Soc.*, 14, 74 (GF-15), (1969).
- [12] H.Z. Cummins and Schoen P.E. (1972), "Linear Scattering from Thermal Fluctuations," in Arecchi and Schultz-DuBois (Eds.), *Laser Handbook*, Vol.2 (p. 1029-1075), North-Holland Publ. Co., Amsterdam.
- [13] P. Benassi, *et al.*, *Phys. Rev. B*, 48(9), 5987-5996, (1993).
- [14] A.I. Ritus, *Tr. Fiz. Inst. Akad. Nauk SSSR*, 137, 3(1982).

- [15] H. R. Carleton, *Amorphous Materials*, eds. R. W. Douglas and Bryan Ellis (Wiley, Interscience, New York, p.103, (1972); *Bull. Am. Phys. Soc.*, 14, 74 (GF-15), (1969).
- [16] K. Matusita *et al*, *J. Non-Cryst. Solids*, 112, 341-346, (1989).
- [17] J. Schroeder, "Brillouin scattering and pockels coefficient in silicate glass," *J. Non-Cryst. Solids.*, 40, 549-566 (1980).
- [18] J.R. Sandercock, *Operator Manual for Tandem Interferometer*, Sept. (1993).
- G-Q. Shen, Z.N. Utegulov, J.P. Wicksted, *Phys. Chem. Glasses*, 43(2), 73-9, (2002).
- [19] . M. Vaughan, *Fabri-Perot Interferometers*, p.214
- [20] K. J. Kao, "Structural Chemistry of Glasses," Elsevier Science Ltd, NY, (2002).
- A.Y.Hamad, J.P.Wicksted, M.R. Hogsed, J.J. Martin, C.A. Hunt and G.S. Dixon, *Phys Rev B*, (2002), 65, 064204-1.
- [21] E. Hecht, *Optics*. 8th ed., (Addision-Wesley, New York,1990), Chap.34.
- [22] G.H. Gangwere, *PhD Thesis*, [Oklahoma State University](#), (1990).

- [23] Miyaki, T. Yoko, J. Jin, S. Sakka, T. Fukunaga, M. Misawa, "Neutron and x-ray diffraction studies of PbO-Ga₂O₃ and Bi₂O₃-Ga₂O₃ glasses," *J. Non-Crys. Solids*, 175, 211-223 (1994).
- [24] F. Miyaki, K. Tadanaga, T. Yoko, and S. Sakka, "Coordination of Ga³⁺ ions in PbO-Ga₂O₃ glasses as determined by ⁷¹Ga NMR," *J. Non-Crys. Solids*, 139, 268-270 (1992).
- [25] J. Schroeder, M. Fox-Bilmont, B G. Pazol, V. Tsoukala, M. G. Drexhage, and O.H. El-Bayoumi, "Rayleigh and Brillouin scattering in heavy metal fluoride glass:intrinsic Rayleigh scattering," *Opt. Eng.*, 24(4), 697-703(1985).
- [26] M. Lveventhal and P. J. Bray, *Phys. Chem. Glasses*, 6, 113 (1965).

①

VITA

SANG HOON PARK

Candidate for the Degree of

Master of Science

Thesis: BRILLOUIN SCATTERING STUDIES IN LEAD BISMUTH GALLATE
BORON GLASSES

Major Field: Physics

Biographical:

Personal Data: Born in Seoul, Korea, October 31, 1975, the son of Hune-Tack Park and Mu-Hea Han.

Education: Graduated from Sang Moon High School, Seoul, Korea, in February 1994: received Bachelor of Science degree in Physics and Bachelor of Engineering degree in Electrical and Computer Engineering from Hanyang University, Seoul, Korea, 2001: completed requirements for the Master of Science degree in Physics from Oklahoma State University in July, 2004.